LA-UR-17-24901

Possible Mechanism for the Generation of a Fundamental Unit of Charge (long version)

J. P. Lestone
Computational Physics Division, Los Alamos National Laboratory
Los Alamos, NM 87545, USA
June 15th, 2017

Abstract

Various methods for calculating particle-emission rates from hot systems are reviewed. Semi-classically derived photon-emission rates often contain the term $\exp(-\varepsilon/T)$ which needs to be replaced with the corresponding Planckian factor of $[\exp(\varepsilon/T)-1]^{-1}$ to obtain the correct rate. This replacement is associated with the existence of stimulated emission. Simple arguments are used to demonstrate that black holes can also undergo stimulated emission, as previously determined by others. We extend these concepts to fundamental particles, and assume they can be stimulated to emit virtual photons with a cross section of $\pi\lambda\!\!\!^{-2}$, in the case of an isolated particle when the incident virtual-photon energy is $< 2\pi mc^2$. Stimulated-virtual photons can be exchanged with other particles generating a force. With the inclusion of near-field effects, the model choices presented give a calculated fundamental unit of charge of 1.6022×10^{-19} C. If these choices are corroborated by detailed calculations then an understanding of the numerical value of the fine structure constant may emerge. The present study suggests charge might be an emergent property generated by a simple interaction mechanism between point-like particles and the electromagnetic vacuum, similar to the process that generates the Lamb shift.

Table of contents

I. Introduction

Despite all the successes of non-relativistic quantum mechanics [HEI25, SCH26] in facilitating our detailed understanding of microscopic (molecular, atomic, and nuclear) phenomena; the enormous success of relativistic quantum mechanics [DIR27] and quantum electrodynamics (QED) [TOM46, SCH48, FEY49, DYS49]; and the more recent standard model of particle physics which enables an understanding of the electro-weak [ERL06], and strong-nuclear [HIN06] forces via quantum field theory (QFT), many unsolved mysteries remain. These mysteries include (but are not limited to): Why does the universe contain leptons and quarks? Why are there three generations of leptons and quarks? Why do the leptons and quarks have their respective masses and charges? Many have pinned their hopes on string theory to answer these questions. However, decades of work on string theory have led to the suggestion that there are $\sim 10^{500}$ possible universes; our universe is one in a much larger multiverse; and that the fundamental constants (standard model parameters) of our universe can only be understood via the anthropic principle (or perturbations thereof). It is possible that the anthropic principle is the key to understanding many of the properties of our universe. However, it is my opinion that this is a modern copout, similar to pre-enlightenment thinking where unexplained phenomena were attributed to a deity or deities.

In 2005 I decided to try and explain why the universe has a fundamental unit of charge of 1.60218×10^{-19} C, and to do this without string theory or the anthropic principle. I am not alone in this desire, and a great many authors have pursued this problem for more than a century, but without success [JEN14]. Most physicists do not think of this problem in terms of the fundamental unit of charge but prefer to think in terms of calculating the dimensionless electromagnetic coupling (fine structure) constant which has been determined by experiment to be α = 0.007297352568 [HAN11]. Many physicists (including myself) have remembered the inverse of this value α^{-1} = 137.0359991. Feynman famously said [FEY85] "all good theoretical physicists put this number up on their wall and worry about it" and "it's one of the greatest damn mysteries of physics: a magic number that comes to us with no

understanding by man." Pauli stated [PAU] that "The theoretical determination of the fine structure constant is certainly the most important of the unsolved problems of modern physics… To reach it, we shall, presumably, have to pay with further revolutionary changes of the fundamental concepts of physics..." This last quote merely reflects the fact that we have not been able to understand the fine structure constant via traditional thinking, and thus it is possible that non-traditional thinking will be required to solve this problem. Perhaps this non-traditional thinking involves string theory and/or the anthropic principle. My gut feelings say no. Unfortunately, the need for non-traditional thinking appears to have recently relegated the pursuit of a theoretical understanding of the fine structure constant to the realm of crackpot science, in the minds of some in main stream physics. I have experienced this first hand. I have given two seminars on this topic to LANL audiences with mixed reviews. The favorability of the responses appeared to be inversely proportional to the audience member's knowledge of QFT and/or black holes. Potential readers should thus be aware that on these topics I might not know what I am talking about.

One of the problems with trying to calculate particle force coupling constants is how to start if you believe fundamental particles are point-like with no internal structure. One possibility is to use string theory which provides internal structure, and lots of it if higher dimensional spaces are invoked. This plethora of internal structure lends itself to the possibility that string theory might solve many great challenges in one foul swoop. My personal breakthrough came in 1988 when I realized that Hawking radiation [HAW74] is a mechanism that enables one to calculate a coupling between electromagnetic radiation (photons) and naked black holes, which had previously been believed to be cold point-like objects. This lends itself to the possibility that if fundamental point-like particles (like leptons) have some of the properties of charge-less black holes then a particle-photon coupling constant could be calculated, and thus charge might be an emergent property associated with micro quantum black holes. At that time my suggestion that Hawking radiation might be the key to understanding the existence of charge was met with firm rejection. Co-workers more senior, and more experienced then I knew that fundamental particles could not be black holes. Perhaps this is true, but I do not have the required general relativity and QFT skill sets to understand these arguments. The need to focus on my PhD, followed by two postdoctoral fellowships, an assistant professorship, and then starting a career in nuclear safeguards meant that thoughts of black holes needed to be placed on the backburner. However, after obtaining more stable employment in 2004, the corresponding increase in free time led me to start rethinking old ideas. This generated a series of thoughts on the possible connection between charge and black holes. I knew this work was not of a quality to justify publication in a referred journal. Hoping to inspire someone else brighter than I to pursue the idea further, I placed my thoughts on the arXiv over the 2007-2009 time frame [LES07]. In hindsight, some of my 2007-2009 arXiv submissions are terrible.

In 2015 I made a breakthrough when I realized near-field corrections were needed when considering the virtual exchange of photons between a pair of micro black holes, and have finally crossed the threshold where publication is how warranted. Before publishing, I sort and received feedback from a few of the great mind in physics from both the 20^{th} and 21^{st} centuries, who received a concise version of this work via private communications. This feedback has been polite but blunt with comments like "I do not understand a single assumption made." Comments like these are likely quick responses which are really saying; please do not bother me with your work anymore. However, I have wondered if the lack of understanding is true, and perhaps some theorists do not have a good understanding of how to deal with collective objects containing significant degrees of freedom, and how simple rules of collective systems appear to be applicable to a wide variety of objects from atomic nuclei operating on time scales of $\sim 10^{-21}$ s, to stars and globular star clusters operating on time scales of billions of years.

As a nuclear physicist I am used to dealing with the complexity of excited nuclei containing many internal degrees of freedom, and the powerful methods for calculating the properties of these complex objects. For example, a modern computational theorist highly trained in the details of nucleon-nucleon reactions and the complex physics of Pauli blocking might embark on a study of neutron emission using microscopic physics occurring inside an excited nucleus to model the production of neutrons with enough energy to escape the strong-nuclear force that holds the nucleons together. However, the experienced practitioner uses the properties of how neutrons are absorbed by nuclei to infer the neutron emission properties via powerful time symmetry and/or thermodynamic agreements. Similar methods can be applied to the problem of photon emission from black holes, once a temperature has been assigned. If these methods work for black holes which were once assumed to be cold point-like objects, then why not apply these methods to the problem of the fundamental-particle photon coupling?

Trained as an experimentalist in low-energy heavy-ion reactions specializing in fusion-fission reactions [LES90], I am used to working in a field for which there is no first-principles calculable theory, and thus used to making suggestions of semi-classical reaction mechanisms guided by experimental observations [e.g. LES08]. In general, these suggestions are not at first graded by one's ability to perform a detailed theoretically justify, but by the computational consequences of the reaction mechanism to reproduce experimental observations. Examples of the use of this methodology are common place in nuclear physics [e.g. LEI90, LES97, LES09]. This method of making progress may seem clumsy to theorists in fields with well-established first principle calculable theories. However, I remind the reader that examples abound in the early development of quantum mechanics and include Planck's suggestion that electromagnetic radiation at a frequency ν can only be emitted and absorbed in integer multiples of energy equal to $h\nu$ [PLA01]; Einstein's suggested reaction mechanism for the production of photoelectrons [EIN05]; and Bohr's suggestion that hydrogen atomic electron orbits are circular with orbital angular momentum values equal to positive integer multiples of $\hbar$ [BOH13].

In the present manuscript I attempt to find an explanation for the existence of a fundamental unit of charge of 1.60218×10^{-19} C. The method applied is to find relatively simple rules for a reaction mechanism associated with the exchange of photons between a pair of particles that lead to a repulsive force that can be characterized by an effective charge close to the known fundamental charge. Simple mechanisms that lead to an effective charge close to the known fundamental charge should be presented to a wider audience for review and consideration. I here present a detailed and long discussion of my proposed mechanism. This includes a discussion of: some previously worked examples where relatively simple semi-classical arguments lead to an understanding of some complex phenomena; techniques used to understand complex emission processes by studying the simpler absorption process; followed by a detailed discussion of my proposed mechanism for the generation of a fundamental unit of charge. The reader should be aware that there are gaps in my work on the fundamental unit of charge (fine structure constant) that are filled by speculative suggestions that I cannot justify at the present time, except they lead to favorable calculational outcomes.

This document is written at a level where I hope it is a relatively easy, though long, read for those with a Bachelor's degree with a major in physics, and with significant parts understandable to talented students with an excellent high-school physics education. To meet this hope, instead of relying on references to journal articles and books, when appropriate, I have tried to keep this document relatively self-contained by repeating some common proofs and/or derivations. If one wants to cut to the chase I recommend you jump to section V. However, do not pass a negative judgement until reading sections III and IV, as these sections demonstrate the success of several semi-classical methods capable of giving results in agreement with more complex quantum theory and review semi-classical methods that can be used to calculate particle-emission rates.

II. Importance of the fine structure constant

The electrostatic force between two charged leptons or a charged lepton and proton separated by a distance d can be expressed as

$$F = \pm\frac{e^2}{4\pi\varepsilon_o d^2} = \pm\frac{\alpha\hbar c}{d^2}, \tag{II.1}$$

where $e = 1.602177\times10^{-19}$ C is the fundamental unit of charge [MOH15]. The fine structure constant, α, can be defined relative to the elementary charge e via

$$e^2 = \alpha\hbar c\, 4\pi\varepsilon_o. \tag{II.2}$$

The fine structure constant was first introduced and used by Sommerfield [SOM16] for defining the separation between closely spaced photon-emission lines (fine structure) in atomic spectroscopy. However, since then, it has been found to have a central importance in QED, and many formulas associated with atomic properties can be expressed more simply with the use of α. For example: the binding energy of the hydrogen atom is $\alpha^2 m_e c^2/2$, where m_e is the electron's mass; the corresponding average separation between the electron and the proton is the Bohr radius $a_0 = \lambda\!\!\!^{-}_C/\alpha$, where $\lambda\!\!\!^{-}_C = \hbar/(m_e c)$ is the reduced Compton wavelength; the corresponding average electron speed is $v = \alpha c$; the characteristic length scale for photon-electron interactions is the classical electron radius $r_e = \alpha\lambda\!\!\!^{-}_C$; and the magnetic moment of the electron is $\mu_e = 1+\alpha/(2\pi)$ Bohr magnetons (to 2nd order in QED). Despite the central importance of the value of α to all atomic process and thus QED, and the many attempts to understand it from a theoretical perspective [JEN14], there is still no accepted theory to explain its value and the corresponding elementary charge e.

III. Usefulness of semi-classical approximations of hydrogen

Since the advent of quantum theory, semi-classical approximations have been used to obtain an understanding of a wide variety of observed phenomena. These approximations often have significant deficiencies, while capturing some essence of the phenomena and reproducing some key experimental observables. The main use of semi-classical approximations has, in general, been twofold. The most important of these has been as a stepping stone to a more complete theory. The other is as teaching tools to explain some complex processes easily to students before their mathematical skills have developed to the point where the more complex theory can be understood. The full list of useful semi-classical approximations is too massive to even partially cover here. The complexity of nuclear systems, along with the lack of a first-principle calculable model of nuclear phenomena, has led to the widespread use of semi-classical models in this field. Many of these models are understandable by undergraduate students and used to explain nuclear masses, alpha-decay rates, fission processes, nuclear shell structure, and collective rotations, to name just a few. In this document, we highlight only a few semi-classical models associated with the hydrogen atom, and the complexity of particle emission from various objects (in the next section). The first two (sections III.A and III.B) are associated with the hydrogen atom and not directly related to the main theme of this document, but are presented to remind the reader that simple but incomplete theories have been useful as an intermediate step to introduce new ideas which, in time, lead to a more complete theory. The discussion on the Lamb shift (section III.C) is of great importance because it is an example of how the interaction of point particles with the electromagnetic vacuum manifests itself as an experimentally observable quantity. In a later section, we will suggest that the charge of leptons is an emergent property of a pair of particles interacting through the electromagnetic vacuum via a process similar to the Lamb shift. The Lamb shift is associated with the

emission and reabsorption of virtual photons by a single electron. In a system consisting of two electrons, not only are virtual photons emitted and reabsorbed by the same electron, but they can be emitted by one electron and absorbed by the second. This exchange generates a repulsive force that defines a charge of ~10^{-19} C.

III.A Bohr theory of hydrogen

Following in the footsteps of Planck and Rutherford, Bohr in 1913 [BOH13] suggested a mechanism by which the energy and motion of the electron in the hydrogen atom could be limited to discrete orbitals or quantum states. The central assumptions are that the electron moves in an electric field associated with a point-like but massive particle of the opposite charge (the proton); and the electron's motion is in classical circular orbits but with fixed values of angular momentum given by $n\hbar$, where n is a positive integer. The acceleration of an electron due to its interaction with the proton is $a = \alpha\hbar c/(m_e r^2)$ and thus, for circular orbits, the electron's velocity is given by $v = (ar)^{1/2} = [\alpha\hbar c/(m_e r)]^{1/2}$. The corresponding orbital angular momentum is $(\alpha\hbar c m_e r)^{1/2}$. Squaring this value and setting it equal to $(n\hbar)^2$ gives the allowable radii of electron orbits as

$$r = \frac{n^2\hbar c}{\alpha m_e c^2} = \frac{n^2 \lambda\!\!\!^{-}_{\mathrm{C}}}{\alpha}. \tag{III.A.1}$$

The corresponding calculated energy of the electron is obtained by summing its kinetic energy to its potential energy

$$E = \frac{mv^2}{2} - \frac{\alpha\hbar c}{r} = \frac{\alpha\hbar c}{2r} - \frac{\alpha\hbar c}{r} = \frac{-\alpha^2\hbar c}{2n^2 \lambda\!\!\!^{-}_{\mathrm{C}}} = \frac{-\alpha^2 m_e c^2}{2n^2} = \frac{-13.6\ \mathrm{eV}}{n^2}, \tag{III.A.2}$$

in agreement to the observed properties of the hydrogen atom. The Bohr model of the atom has significant limitations and incorrectly predicts the angular momentum of the orbits. However, it clearly demonstrated that the Rutherford theory of the atom in conjunction with a quantization of the electron's angular momentum was on the right track. It took another decade to realize that the circumferences of the Bohr orbits are integer multiples of the electron's De Broglie wavelengths given by $\lambda = h/p$. This helped cement the idea that particle wave mechanics was central to the understanding of atom phenomena and led the way for the Schrödinger equation [SCH26].

III.B Uncertainty principle and the hydrogen atom

The uncertainty principle in one dimension states that the product of the uncertainties in position and momentum must be equal to or larger than $\hbar/2$. Therefore, for an electron orbiting a distance r from a proton in three physical dimensions, it might be reasonable to assume that it will have a quantum mechanically induced momentum of $p = a\hbar/r$. The smaller the orbit, the larger the quantum mechanically induced momentum. Initially, we assume the size of the proportionality constant a, is unknown. The energy of the hydrogen atom can then be expressed as a function of the proton-electron separation r

$$E = \frac{a^2\hbar^2}{2m_e r^2} - \frac{\alpha\hbar c}{r}. \tag{III.B.1}$$

If we assume the ground state of the hydrogen atom corresponds to the minimum in Eq. (III.B.1) with respect to r, then we can obtain the Bohr radius a_0 via

$$\frac{\partial E}{\partial r} = \frac{\alpha\hbar c}{r^2} - \frac{a^2\hbar^2}{m_e r^3} = 0 \quad \text{and thus} \quad a_0 = \frac{a^2\hbar}{\alpha m_e c}. \tag{III.B.2}$$

This gives the correct result if we assume $a = 1$. The corresponding ground state energy is

$$E = \frac{\hbar^2}{2m_e a_0^2} - \frac{\alpha\hbar c}{a_0} = \frac{-\alpha^2 m_e c^2}{2}\ , \tag{III.B.3}$$

in agreement with Eq. (III.A.2) with $n = 1$, with a kinetic energy of 13.6 eV and a potential energy of –27.2 eV. The semi-classical formulism presented in this section cannot be used to give the energy of the excited states like the Bohr model does, but can be used to introduce the mechanism for the formation of molecules and how atoms resist compression.

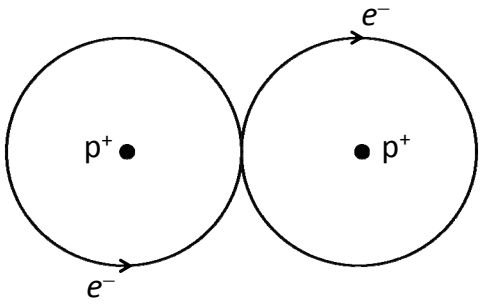

Fig. III.B.1. Schematic representation of the H_2^+ and H_2 molecules.

To estimate the binding energy of H_2^+ and H_2 we assume these molecules can be approximately represented as shown in Fig. III.B.1. For both molecules, we assume the electron(s) form spherical shells with radii a_0 around each proton and thus the two protons are separated by ~$2a_0$. In the case of H_2^+ the single electron relaxes along the molecule's symmetry axis. In the hydrogen atom the 13.6 eV of kinetic energy can be considered to be in three equal units of ~4.5 eV, one unit for each of the three spatial dimensions. The presence of the additional proton causes the available space for one of the dimensions to increase by a factor of ~2. The corresponding quantum-mechanically induced momentum is halved, and thus the kinetic energy associated with this direction is reduced by a factor of four to ~1.1 eV. This reduction in the kinetic energy along the symmetry axis from ~4.5 eV to ~1.1 eV causes a reduction in the system's energy by ~3.4 eV relative to that associated with a hydrogen atom and a well-separated proton. This simple estimate of a binding energy of 3.4 eV for H_2^+ is ~26% higher than the experimental value of 2.8 eV (at room temperature). In the case of the H_2 molecule, two electrons are involved and thus the simple estimate of the corresponding binding energy is doubled to 6.8 eV. This is ~50% higher than the experimental value of 4.5 eV. The major reason for this discrepancy is that the H_2 bond is strong enough to reduce the bond length to ~$1.4a_0$. This gives a reduction of the kinetic energy of each electron in the direction along the symmetry axis from 4.5 eV to ~2.3 eV. This leads to an estimated H_2 molecular binding energy of 4.4 eV. Of course, a detailed analysis of the true nature of the H_2^+ and H_2 molecules is more complex, with important issues related to electron spin, Pauli blocking, and symmetric and anti-symmetric wave functions. However, the simple method used here gives rough estimates for the binding energies, and demonstrates the main mechanism behind molecular bonding is the uncertainty principle and the corresponding reduction in the kinetic energy of electrons when they can relax spatially in the direction of a bond axis.

The work done to compress gas at a pressure P by a volume dV is given by $W = PdV$. The work required to change the radius of a hydrogen atom can be determined using Eq. (III.B.2) and expressed as

$$\frac{\partial E}{\partial r}\partial r = \left(\frac{\alpha\hbar c}{r^2} - \frac{\hbar^2}{m_e r^3}\right)\partial r = -PdV. \qquad \text{(III.B.4)}$$

Setting the effective volume occupied by each close packed atom to $V \sim 4\pi r^3/3$ leads to the expression

$$P \sim \frac{1}{4\pi r^4}\left(\frac{\hbar^2}{m_e r} - \alpha\hbar c\right) = \frac{\alpha\hbar c}{4\pi r^4}\left(\frac{a_0}{r} - 1\right) = \left(\frac{a_0}{r} - 1\right) 2357\ \text{GPa}. \qquad \text{(III.B.5)}$$

The pressure in the center of the Earth is ~365 GPa. Via Eq. (III.B.5) this pressure can be obtained by a 10% reduction in the radii of the atoms in the Earth's core. This demonstrates that the earth beneath your feet is held up by the uncertainty principle. The pressure in the center of Jupiter is estimated to be ~4000 GPa. This is maintained by a reduction in size of the hydrogen atoms present there of $r/a_0 \sim 0.7$ [obtained via Eq. (III.B.5)]. This in turn, corresponds to a hydrogen-core density of ~ 4 g/cc in agreement with more detailed calculations.

III.C Hydrogen Lamb shift

According to the Dirac equation (without including vacuum physics), the hydrogen $2s_{1/2}$ and $2p_{1/2}$ levels should be degenerate (have the same energy). This is a consequence of an assumed pure inverse-square-law Coulomb force between the electron and the proton. There are many reasons why the true interaction will not follow a perfect inverse-square law at small proton-to-electron length scales. These include the finite size of the proton, vacuum polarization associated with virtual electron-positron pairs [UEH35], and a possible intrinsic fuzziness of the electromagnetic interaction involving electrons on small length scales. In 1947 Lamb and Retherford [LAM47], using microwaves, clearly demonstrated that the hydrogen $2s_{1/2}$ level sits ~1000 MHz above the $2p_{1/2}$ level. Bethe demonstrated in the same year [BET47] that this observation was predominantly due to the electromagnetic vacuum interacting with the electron. A more modern measurement of the Lamb shift is 1057.85 MHz [BRO92]. The corresponding QED calculation is 1057.86 MHz [BRO92].

Welton [WEL48, BJO64] obtained a simple qualitative description of the Lamb shift and we repeat this derivation here. The number density of electromagnetic modes is as given by Eq. (IV.B.4). In the vacuum ground state, each oscillator mode has an energy $\hbar\omega/2$, and thus we can write the energy density of the vacuum as

$$\rho_E(\varepsilon)d\varepsilon = \frac{1}{2\pi^2}\frac{\varepsilon^3 d\varepsilon}{\hbar^3 c^3} = \frac{\varepsilon_0 < E^2 >}{2} + \frac{< B^2 >}{2\mu_0} = \varepsilon_0 < E^2 >, \qquad \text{(III.C.1)}$$

where $\varepsilon = \hbar\omega$. The motion (oscillation) of an electron in a fixed frequency electromagnetic field can be described by

$$\ddot{x} = \frac{eE}{m} = \frac{e}{m}E_{\max}\sin(x/\lambda\!\!\!^{-})\sin(\omega t) \ \text{ and thus } x = \frac{-e}{m\omega^2}E_{\max}\sin(x/\lambda\!\!\!^{-})\sin(\omega t) \ \text{ and}$$
$$< x^2 > = \frac{e^2}{m^2\omega^4}\frac{E_{\max}^2}{4} = \frac{e^2 < E^2 >}{m^2\omega^4}, \qquad \text{(III.C.2)}$$

where E is the instantaneous electric field, $E_{\max}$ is the maximum electric field associated with the mode with an angular frequency of ω, and $<E^2>$ is the mean-square electric field averaged over space and time. Combining Eq.s (III.C.1) and (III.C.2) gives

$$< x^2 > = \frac{e^2\varepsilon^3 d\varepsilon}{m^2\omega^4\varepsilon_0 2\pi^2\hbar^3 c^3} = \frac{4\alpha\hbar^2 d\varepsilon}{m^2 2\pi c^2 \varepsilon} = \frac{2\alpha\lambda\!\!\!^{-2}_{C}}{\pi}\frac{d\varepsilon}{\varepsilon}. \qquad \text{(III.C.3)}$$

In the case of randomly orientated and phased vacuum modes we can express the root-mean-square spread in the electron's location associated with its interaction with the vacuum as [BJO64, pg. 60]

$$< \delta r^2 >= \frac{2\alpha \lambda\!\!\!^{-2}_{C}}{\pi} \int \frac{d\varepsilon}{\varepsilon} . \qquad \text{(III.C.4)}$$

The integral in Eq. (III.C.4) diverges if the lower limit is zero and/or if the upper limit is infinite. Therefore, in order to obtain a finite result, there needs to be both lower- and upper-energy cutoffs. The high-energy cutoff associated with the relativistic structure of the electrons will be ~mc^2 [BJO64, pg. 60]. There must be a low-energy cutoff, because wavelengths very much larger than the characteristic size of the system (approximately the Bohr radius) cannot shake the bound-electron independent of the proton. The corresponding low-energy cutoff is often assumed to be ~ αmc^2 [BJO64, pg. 60], and Eq. (III.C.4) can be written as

$$< \delta r^2 >= \frac{2\alpha \lambda\!\!\!^{-2}_{C}}{\pi} \int_{\alpha}^{1} \frac{d\varepsilon}{\varepsilon} = \frac{2\alpha \ln(1/\alpha) \lambda\!\!\!^{-2}_{C}}{\pi} \text{ and thus } < \delta r^2 >^{1/2} = \sigma_r \sim \frac{\lambda\!\!\!^{-}_{C}}{6.61} . \qquad \text{(III.C.5)}$$

From the Darwin term in the Dirac equation it follows that the hydrogen Lamb shift is [BJO64, pg. 59]

$$\Delta E_n = \frac{2\pi}{3} \alpha \hbar c < \delta r^2 > |\psi_n(0)|^2 . \qquad \text{(III.C.6)}$$

The corresponding upward shift in the hydrogen 2*s* level is

$$\Delta E_{2s} = \frac{2\pi}{3} \alpha \hbar c \frac{2\alpha \ln(1/\alpha) \lambda\!\!\!^{-2}_{C}}{\pi} (\frac{\alpha}{2\lambda\!\!\!^{-}_{C}})^3 \frac{4}{4\pi} = \frac{\alpha^5 \ln(1/\alpha)}{6\pi} mc^2 = 667.4 \text{ MHz} . \qquad \text{(III.C.7)}$$

For those not familiar with the Dirac equation, this derivation is not very transparent, so we also show a derivation of (III.C.7) using first-order perturbation theory where the shift in the energy of a given state is

$$\Delta E = \int \psi \cdot \Delta V \cdot \psi \, dv \qquad \text{(III.C.8)}$$

where ΔV is the perturbation of the potential. Invoking the central-limit theorem and the large number of randomly orientated and phased vacuum modes, the blurriness of the electron's charge associated with its interaction with the electromagnetic vacuum will be Gaussian with a standard deviation of σ_r [see Eq. (III.C.5)]. However, the size of the Lamb shift can be shown to depend only on the root-mean-square spread of the charge blurriness, and not on the details of the shape of the distribution (an exercise for the reader). Given this, we chose the simplest distribution of a delta spike at a radius of σ_r to evaluate the Lamb shift. This choice causes ΔV to be zero for $r > \sigma_r$ and $\Delta V = \alpha\hbar c(1/r - 1/\sigma_r)$ for $r < \sigma_r$, and enables us to write the shift in the hydrogen 2s level as

$$\Delta E_{2s} = \int_0^{\sigma_r} \left(\frac{\alpha}{2\lambda\!\!\!^{-}_{C}} \right)^3 \frac{4}{4\pi} (1 - \frac{\alpha r}{2\lambda\!\!\!^{-}_{C}})^2 \exp(\frac{-\alpha r}{\lambda\!\!\!^{-}_{C}}) \alpha \hbar c (\frac{1}{r} - \frac{1}{\sigma_r}) 4\pi r^2 dr . \qquad \text{(III.C.9)}$$

Given that $\sigma_r << \lambda\!\!\!^{-}_{C}$, the radial dependences of the wave function can be set constant over the range of the integral in Eq. (III.C.9). Switching to a radial unit of $\lambda\!\!\!^{-}_{C}$, and using Eq. (III.C.5) enables us to rewrite Eq. (III.C.9) as

$$\Delta E_{2s} = \frac{mc^2\alpha^4}{2} \int_0^{\sigma_r/\lambda\!\!\!^{-}_{C}} (r - \frac{r^2}{\sigma_r/\lambda\!\!\!^{-}_{C}}) \, dr = \frac{mc^2\alpha^4}{12} \left(\frac{\sigma_r}{\lambda\!\!\!^{-}_{C}} \right)^2 = \frac{mc^2\alpha^4}{12} \frac{2\alpha \ln(1/\alpha)}{\pi} = \frac{\alpha^5 \ln(1/\alpha)}{6\pi} mc^2 , \qquad \text{(III.C.10)}$$

as given in Eq. (III.C.7). The corresponding value of 667.4 MHz is significantly different from the experimental value of 1058 MHz. This does not seem to have given other authors much angst, and the difference between Eq. (III.C.10) and the corresponding experimental value appears to generally be

assumed to be associated with the various approximations needed to obtain Eq. (III.C.4). One must be careful not to read too much into simplified calculations, but equally careful to consider the possibility that factors of 2, π, and/or 2π have been misplaced when obtaining the low- and high-energy cutoffs in Eq. (III.C.5). Such changes can be attributed to mixing up lengths that should be assigned to a circumference and/or radius and/or a diameter. For example, it would not be surprising if, on noticing that Planck's constant has units of angular momentum, that Bohr first considered the possibility that angular momentum might be quantized in units of h. On noticing that this model fails, it would not be a surprise if an astute examiner would discover that quantizing in units of ħ appeared satisfactory and boldly suggested this instead. Such adjustments should not be viewed as numerology, but considered as theoretical adjustments guided by experiment. Here, we apply this possibility to the length scale assumptions used to obtain the energy cutoffs in Eq. (III.C.5).

In section VII.C, arguments are presented that the high-energy cutoff is not at mc^2 but rather at $2\pi mc^2$. This increases the calculated shift in the hydrogen $2s$ level by $[\ln(2\pi)+\ln(1/\alpha)]/\ln(1/\alpha)$ giving ΔE_{2s}=916.7 MHz. If we consider the relevant length scale for the low-energy cutoff is half the circumference of the lowest Bohr orbital (instead of the Bohr radius), then the low-energy cutoff becomes $\alpha mc^2/\pi$. Using the cutoffs discussed in this paragraph gives

$$<\delta r^2>=\frac{2\alpha\lambda\!\!\!^{-2}_{C}}{\pi}\int_{\alpha/\pi}^{2\pi}\frac{d\varepsilon}{\varepsilon}=\frac{2\alpha\ln(2\pi^2/\alpha)\lambda\!\!\!^{-2}_{C}}{\pi}\ \text{and}\ \Delta E_{2s}=\frac{\alpha^5\ln(2\pi^2/\alpha)}{6\pi}mc^2=1071.97\ \text{MHz}. \quad \text{(III.C.11)}$$

The corresponding root-mean-square spread in the electron's location is $<\delta r^2>^{1/2}\sim \lambda\!\!\!^{-}_{C}/5.219$. Several other effects need to be added to Eq. (III.C.11) before making a quantitative comparison with the experimental value of 1057.85 MHz. These include the shift in the $2s$ level associated with the polarization of the vacuum [UEH35]

$$\Delta E_{2s}(\text{vacuum polarization})=\frac{\alpha^5}{30\pi}mc^2=-27.13\ \text{MHz}; \quad \text{(III.C.12)}$$

the shift in the $2p_{1/2}$ level [BET50, KAR52]

$$\Delta E_{2p_{1/2}}=\frac{\alpha^5}{6\pi}(0.030-\frac{1}{8})mc^2=-12.89\ \text{MHz}; \quad \text{(III.C.13)}$$

and the small correction due to the proton's size [KEM33]

$$\Delta E_{2s}(\text{proton's size})=\frac{\alpha^5}{6\pi}\frac{\pi}{2\alpha}\left(\frac{0.85\ \text{fm}}{\lambda\!\!\!^{-}_{C}}\right)^2mc^2=0.14\ \text{MHz}. \quad \text{(III.C.14)}$$

Adding these terms together gives the prediction for the difference in energy of the hydrogen $2s_{1/2}$ and $2p_{1/2}$ levels (the Lamb shift) of

$$\Delta E_{2s_{1/2}}-\Delta E_{2p_{1/2}}=\frac{\alpha^5mc^2}{6\pi}\left\{\ln(2\pi^2/\alpha)-\frac{3}{40}-0.030+\left(\frac{0.85\ \text{fm}}{\lambda\!\!\!^{-}_{C}}\right)^2\right\}=1057.87\ \text{MHz}. \quad \text{(III.C.15)}$$

Given the approximations made, the level of agreement with experiment is stunning, but possibly fortuitous. However, I like to believe that the success of Eq. (III.C.15) is due to the more prudent choice of cutoff energies, and the fact that simple semi-classical methods can sometimes give accurate results as demonstrated by the Bohr theory of the hydrogen atom.

IV. Understanding emission via absorption

In 1917 Einstein [EIN17] showed spontaneous emission, absorption, and stimulated emission are intimately connected; in particular, that the cross section for the absorption of a photon of energy $\varepsilon = \varepsilon_2 - \varepsilon_1$ by a system making a transition from state 1 to 2, is identical to the cross section for a photon of the same energy to stimulate the system in state 2 to make the transition to state 1, with the emission of the corresponding photon. These processes are depicted in Fig. IV.1. Spontaneous emission can then be viewed as the process by which virtual-vacuum photons stimulate sites of excitation to de-excite (see section IV.D.1). Another key finding of Einstein's 1917 paper, is that for a system in thermodynamic equilibrium at temperature T, the ratio of stimulated to spontaneous emission of photons of energy ε is given by $[\exp(\varepsilon/T)-1]^{-1}$. The connection between spontaneous emission, absorption, and stimulated emission is a universal property of matter, including atoms, molecules, crystals, and nuclei. More recently, these connections have been found to apply to black holes [BEK77]. In this manuscript, we extend some of these properties to fundamental particles. This extension leads to a straightforward mechanism for the storage of the rest-mass energy of particles in the surrounding cloud of virtual photons. The exchange of these virtual photons between particle pairs generates a force that defines a universal unit of charge of $\sim 10^{-19}$ C. Before applying the concept of stimulated emission to fundamental particles, it pays to first review some of the methods by which we can calculate the emission of photons by collective objects (those made from multiple fundamental particles).

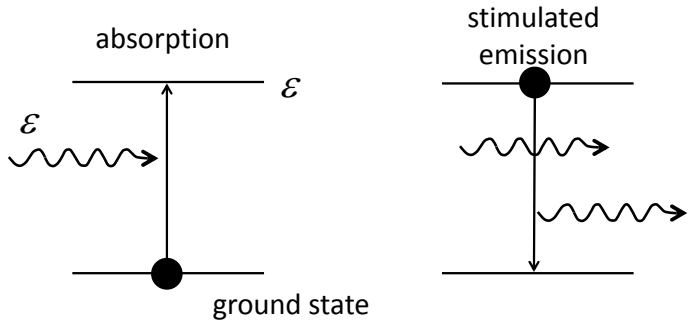

Fig. IV.1. Representations of photon absorption and stimulated emission.

IV.A Weisskopf emission of neutrons from a hot nucleus

In 1937 Weisskopf [WEI37] introduced a clever method for assessing the emission of a given particle from a hot object if the corresponding object-particle absorption cross section is known. As done by Weisskopf, we use this method in this section to estimate the rate of neutron emission from a hot nucleus at temperature T. We consider the nucleus and a single neutron in a cube of volume V with side length L. For simplicity, we at first only consider motion of the neutron perpendicular to two sides of the cube and parallel to the others. The corresponding transit time across the cube will be $t = L/v$ where v is the velocity of the neutron. The probability that the neutron will be absorbed on a single random transit is $P = \sigma_a/L^2$ where σ_a is the neutron-nucleus absorption cross section. The rate of absorption is thus $R_a = P/t = \sigma_a \cdot v/V$. A more detailed analysis with randomly orientated velocities gives the same result. If an ensemble of excited nucleus configurations, and an ensemble of single-nucleus plus single-neutron configurations are in thermodynamic equilibrium, then the relative numbers in each of these ensembles will be proportional to the corresponding number of states available to each configuration. We denote these by the number of emission states n_e, and the number of capture states n_c. The number of emission

states associated with the nucleus can be obtained using the Boltzmann factor of $\exp(-\Delta E/T)$ for the relative reduction of states associated with the removal of an energy ΔE, and given by $n_e(\text{nucleus})=n_c\cdot\exp(-\Delta E/T)$, where ΔE is equal to the sum of the neutron-binding energy of the parent nucleus, B_n, and the kinetic energy of the emitted neutron, ε.

The total number of states available to the emission configuration is the product of those associated with the nucleus (given above) and those associated with the emitted particle, $n_e(\text{particle})$. The quantum state of a non-spinning particle in a cube is denoted by the three quantum numbers n_x, n_y, n_z. These each define an integer number of half wavelengths equal to the side length L. The corresponding wavelengths and momenta components are $\lambda_i=2L/n_i$ and $p_i=h/\lambda_i=n_i\cdot h/(2L)$, respectively, with $i=x$, y, and z, and all three n_i capable of being any positive integer, 1, 2, 3, …∞. The energy of a neutron (particle) in a given state is given by $\varepsilon(n_x,n_y,n_z)=(p_x^2+p_y^2+p_z^2)/(2m_n)=(n_x^2+n_y^2+n_z^2)\pi^2\hbar^2/(2m_nL^2)$, where m_n is the mass of the neutron. The set of coordinates (n_x,n_y,n_z) defines a vector of length $R=(n_x^2+n_y^2+n_z^2)^{1/2}$, and enables us to rewrite $\varepsilon(n_x,n_y,n_z)=R^2\pi^2\hbar^2/(2m_nL^2)$ and $d\varepsilon/dR=R\pi^2\hbar^2/(m_nL^2)$. The possible states (n_x,n_y,n_z) uniformly occupy the 1/8 of a 3-dimensional space where all coordinates are positive with a density of one point per unit volume. In the limit of a very large cube where even the long wavelengths correspond to large n_i values, the number of particle states within the energy range from ε to $\varepsilon+d\varepsilon$ can thus be expressed as

$$\rho_e(\varepsilon)d\varepsilon=\frac{1}{8}4\pi R^2dR=\frac{\pi}{2}R^2\frac{m_nL^2d\varepsilon}{R\pi^2\hbar^2}=\frac{\pi}{2}\frac{Rm_nL^2}{\pi^2\hbar^2}d\varepsilon=\frac{\pi}{2}\frac{L\sqrt{2m_n\varepsilon}}{\pi\hbar}\frac{m_nL^2}{\pi^2\hbar^2}d\varepsilon=\frac{V}{4\pi^2}\left(\frac{2m_n}{\hbar^2}\right)^{3/2}\varepsilon^{1/2}\,d\varepsilon\,. \quad \text{(IV.A.1)}$$

If the particle has a spin s, then this result must be multiplied by $2s+1$ to include the number of spin orientations. For example, this generates a factor of two for $s=1/2$ neutron emission.

If we had an ensemble of n_c capture configurations with nuclei, each in their own cubes, we must have a corresponding ensemble of $n_c\cdot\exp(-\Delta E/T)\cdot\rho_e(\varepsilon)d\varepsilon$ emission configurations with de-excited nuclei, each in their own cubes with an emitted neutron, for each possible neutron-energy range from ε to $\varepsilon+d\varepsilon$. The rate of converting emission configurations into capture configurations is given by $\sigma_a\cdot v/V\cdot n_c\cdot\exp(-\Delta E/T)\cdot\rho_e(\varepsilon)d\varepsilon$. This must be equal to the rate of converting capture configurations into emission configurations, $n_c\cdot R_e(\varepsilon)d\varepsilon$. The probability per unit time per unit energy for emission is thus given by

$$R_e(\varepsilon)=\sigma_a\frac{v}{V}\exp(-\Delta E/T)\rho_e(\varepsilon)=(2s+1)\sigma_a\sqrt{\frac{2\varepsilon}{m_n}}\frac{1}{4\pi^2}\left(\frac{2m_n}{\hbar^2}\right)^{3/2}\varepsilon^{1/2}\exp(-B_n/T)\exp(-\varepsilon/T)$$

$$=\frac{(2s+1)\sigma_am_n}{\pi^2\hbar^3}\exp(-B_n/T)\cdot\varepsilon\exp(-\varepsilon/T)\,. \quad \text{(IV.A.2)}$$

Integrating over all possible emission kinetic energies gives the final neutron-emission rate of

$$R_e=\frac{(2s+1)\sigma_am_n}{\pi^2\hbar^3}\exp(-B_n/T)\cdot\int_0^\infty\varepsilon\exp(-\varepsilon/T)d\varepsilon=\frac{(2s+1)\sigma_am_nT^2}{\pi^2\hbar^3}\exp(-B_n/T)\,. \quad \text{(IV.A.3)}$$

The Maxwellian emission spectrum from Eq. (IV.A.2) corresponds to an average neutron-emission energy of $2T$. As an example of the use of Eq. (IV.A.3), we consider the emission of neutrons from fission fragments in low-energy neutron-induced fission of uranium and plutonium. In these cases, the mean energy of the neutron emission is ~2 MeV in the center-of-mass frame of the fragments. This defines a characteristic temperature for the neutron emission of ~1 MeV. The average fission-fragment atomic mass number is A~120, with a corresponding nuclear radius of ~1.2 fm × $120^{1/3}$ ~ 6 × 10^{-15} m. This, in turn, corresponds to an absorption cross section of σ_a ~ 113 × 10^{-30} m^2. Plugging these values into Eq. (IV.A.3) along with a neutron-binding energy of B_n ~ 6 MeV gives a neutron-emission rate of

$$R_e(\text{fission fragments}) \sim \frac{2\cdot 113\times10^{-30}\,\text{m}^2\cdot 1.7\times10^{-27}\,\text{kg}\,(1.6\times10^{-13}\,\text{J})^2}{10\cdot(1\times10^{-34}\,\text{Js})^3}\exp(-6) \sim 2\times10^{18}\,\text{s}^{-1}.$$

This is slow compared to the time scale for the acceleration of the charged fission fragments (~10^{-20} s), but fast compared to neutron transport and material hydrodynamic time scales (>10^{-8} s). This means the prompt fission neutron emission is slow enough that the vast majority of the prompt-fission neutrons are emitted from fully accelerated fission fragments [LES16], while fast enough that, for neutron transport and hydrodynamic considerations, the prompt-neutron emission can be considered to be instantaneous. Modern nuclear-reaction theory codes [e.g. LES09] do not use the theory of Weisskopf, but the improved Hauser-Feshbach theory [HAU52] based on transition state theory (discussed later). This enables the tracking of the orbital angular momentum of the emitted particles and thus allows for the modification of the spin of the emitting nucleus.

IV.B Weisskopf emission of photons from a black hole

Given the introduction to Weisskopf emission in the previous section, one might expect this section to be relatively short with the photon-emission rate per unit photon energy given by $R_\gamma(\varepsilon)=\sigma_a\cdot c/V\cdot\exp(-\varepsilon/T)\cdot\rho_\gamma(\varepsilon)$. However, this is not the case, given the need to count photon instead of particle configurations, the possibility of needing to include effects associated with stimulated photon emission, and the need to discuss some of the properties of photon black hole interactions.

IV.B.1 Counting photon configurations

Similar to section IV.A on particle emission, we start by considering an evacuated large cube with volume $V=L^3$. However, here we must assume the cube is made of conducting material to provide a boundary condition of no electric field parallel to the surface of the conducting cube walls. The possible photon reduced wavelengths in the $i=x$, y, and z directions are given by

$$\lambda\!\!\!^{-}_{ni} = \frac{\lambda_{ni}}{2\pi} = \frac{2L}{2\pi n_i} = \frac{L}{n_i\pi}. \qquad \text{(IV.B.1)}$$

The angular frequency for a given mode is given by $\omega=c/\lambda\!\!\!^{-}$, where c is the speed of light, and $\lambda\!\!\!^{-}$ is the reduced wavelength of the mode including all three directional components.

To determine the number of possible modes with a fixed frequency (energy) we, for simplicity, first consider modes in the cube, moving along a vector in the xy plane at an angle α to the x axis and β to the y axis (see Fig. IV.B.1). In two dimensions, it is easy to see that $\lambda_x=\lambda/\cos(\alpha)$, $\lambda_y=\lambda/\cos(\beta)$, and $\cos^2(\alpha)+\cos^2(\beta)=1$. The addition of the third dimension introduces the third relationship $\lambda_z=\lambda/\cos(\gamma)$ where γ is the angle of the mode direction to the z axis. The relationship between the three angles defining the direction of the mode is constrained by $\cos^2(\alpha)+\cos^2(\beta)+\cos^2(\gamma)=1$. This relationship and the constraints defined by Eq. (IV.B.1) lead to the results

$$\cos(\theta_i)=\frac{n_i\pi\lambda\!\!\!^{-}}{L} \quad \text{and} \quad R=\sqrt{n_x^2+n_y^2+n_z^2}=\frac{L}{\pi\lambda\!\!\!^{-}}=\frac{\omega L}{c\pi}. \qquad \text{(IV.B.2)}$$

In the limit of a very large cube, where even the long wavelength modes are characterized by large n_i values, the number of modes from R to $R+dR$ is given by $\rho_\gamma(R)dR=\pi R^2dR/2$ (similar to the counting system in section IV.A). Using the relationship between R and ω as given by Eq. (IV.B.2) gives

$$\rho_\gamma(\omega)d\omega = \frac{\pi}{2}\left(\frac{\omega L}{c\pi}\right)^2 \frac{L d\omega}{c\pi} = \frac{\pi}{2}\left(\frac{L}{c\pi}\right)^3 \omega^2 d\omega . \qquad \text{(IV.B.3)}$$

Multiplying by two to include both planes of polarization, and substituting in $\omega=\varepsilon/\hbar$, gives the number of photon states with energies between ε and $\varepsilon+d\varepsilon$

$$\rho_\gamma(\varepsilon)d\varepsilon = \frac{V\varepsilon^2 d\varepsilon}{\pi^2\hbar^3 c^3} . \qquad \text{(IV.B.4)}$$

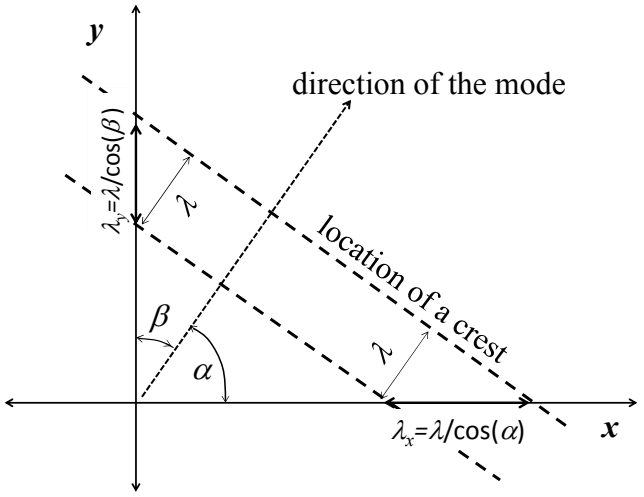

Fig. IV.B.1. Schematic diagram displaying the relationship between the wavelength of a mode in the *xy* plane to the corresponding values of λ_x and λ_y.

IV.B.2 Photon-emission rate

The rate of photon emission per unit energy from an object at temperature T and with an energy independent absorption cross section of σ_a, is thus given by

$$R_\gamma(\varepsilon) = \sigma_a \frac{c}{V}\exp(-\varepsilon/T)\frac{V\varepsilon^2 d\varepsilon}{\pi^2 c^3\hbar^3} = \frac{\sigma_a}{\pi^2 c^2\hbar^3}\varepsilon^2\exp(-\varepsilon/T) . \qquad \text{(IV.B.5)}$$

The above conditions are satisfied by a large black-body object with length scales very much larger than the wavelength of the emitted photons. In this case, an effective surface area, S_A, can be defined by the object's cross-sectional area averaged over all possible orientations multiplied by 4, i.e. $S_A = 4\sigma_a$. The corresponding emission power is given by

$$P_\gamma(\varepsilon)d\varepsilon = \frac{S_A}{4\pi^2 c^2\hbar^3}\varepsilon^3\exp(-\varepsilon/T)d\varepsilon . \qquad \text{(IV.B.6)}$$

Eq.s (IV.B.5) and (IV.B.6) are in disagreement with the known expressions for "real" black-body emission. This situation is easily rectified if one realizes that the one-particle-in-a-box method of Weisskopf can only calculate the emission rate of uncorrelated events involving the spontaneous emission of a single particle. Using the ratio of stimulated emission to spontaneous emission of $[\exp(\varepsilon/T)-1]^{-1}$ (as determined by [EIN17] and discussed earlier) gives the correct total black-body emission power. Including both spontaneous and stimulated emission gives

$$P_\gamma(\varepsilon)d\varepsilon = \frac{S_A}{4\pi^2 c^2\hbar^3}\varepsilon^3\left\{\exp(-\varepsilon/T) + \frac{\exp(-\varepsilon/T)}{\exp(\varepsilon/T)-1}\right\}d\varepsilon = \frac{S_A}{4\pi^2 c^2\hbar^3}\frac{\varepsilon^3 d\varepsilon}{\exp(\varepsilon/T)-1} . \qquad \text{(IV.B.7)}$$

Integrating over all photon energies gives the total emission power

$$P_\gamma = \frac{S_A}{4\pi^2 c^2 \hbar^3}\int_0^\infty \frac{\varepsilon^3 d\varepsilon}{\exp(\varepsilon/T)-1} = \frac{S_A \pi^2 T^4}{60 c^2 \hbar^3} = S_A \sigma_{SB} T^4 , \qquad \text{(IV.B.8)}$$

where the Stefan-Boltzmann constant is given by $\sigma_{SB} = \pi^2/(60c^2\hbar^3)$. Please note that here the temperature is in units of energy and not in degrees. If one wishes to use temperature in degrees Kelvin then the Stefan-Boltzmann constant given above needs to be multiplied by the Boltzmann constant in units of the energy unit per degrees Kelvin raised to the fourth power. The replacement of the exponential term $\exp(-\varepsilon/T)$, in the semi-classically derived photon-emission formula Eq. (IV.B.6), with the Planckian factor $[\exp(\varepsilon/T) - 1]^{-1}$ to obtain the correct result [see Eq. (IV.B.8)], will be a common theme in this manuscript.

IV.B.3 Stimulated photon emission from black holes

Eq.s (IV.B.7) and (IV.B.8) are as given by Hawking for the emission of photons from black holes [HAW74] and apply to all objects at temperature T, with an absorption cross section independent of photon energy. This includes both large black-body objects, and black holes if the absorption process is assumed to be a given by geometric optics. Based on the Planckian factor in Hawking radiation, one might conclude that stimulated emission is occurring. However, it is logical to ask how the spontaneous emission of a single photon from a black hole into the surrounding vacuum can generate any stimulated emission. Fig. IV.B.2 shows a schematic representation of the spontaneous emission of a photon from a black hole, followed by the generation of a stimulated emission. The view on the left is a macroscopic view with no reference to the sites of excitation responsible for the emissions. The large black circle in the left view represents the event horizon of the black hole. In this view the stimulated emission mechanism is a mystery. The view on the right is a microscopic view showing the origin of the photons. The large solid arc is an expanded view of the relevant part of the event horizon. The small black dot is the birth location of a virtual electron-positron pair that both terminate on the black hole (solid curve). During their acceleration a virtual electron-positron pair can spontaneously emit a photon whose information to conserve energy and moment is conveyed back to the black hole via the virtual-particle pair. It is possible for the spontaneously emitted photon to pass near the trajectory of another virtual-particle pair depicted by the dashed curve and the birth location displayed by the open circle in Fig. IV.B.2. Without the presence of the spontaneously emitted photon the other virtual pair (dashed curve) would likely have disappeared without the production of a photon. However, the trajectory of the pair can be viewed as a possible emission source which can be stimulated to emit due to the passage of the spontaneously emitted photon.

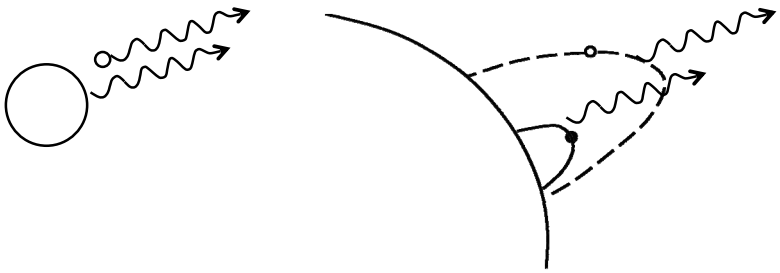

Fig. IV.B.2. Schematic representation of the spontaneous emission of a photon from a black hole, followed by the generation of a stimulated emission. The view on the left is a macroscopic view with no reference to the sites of excitation responsible for the emission (see text). The view on the right is a microscopic view depicting the origin mechanisms (see text).

Given the emission processes depicted in Fig. IV.B.2, the absorption and stimulated emission processes initiated by photons (both real and virtual) incident on a black hole as depicted in Fig. IV.B.3, must also be possible. The large open-black circles in Fig. IV.B.3 depict the event horizons and the small solid circles display the birth locations of virtual electron-positron pairs whose trajectories (dashed curves) terminate on the black holes. The depicted absorption process allows for photons that were not going to cross the event horizon to be absorbed with the virtual pair conveying the necessary energy and momentum conservation back to the black hole's center. The atmosphere of black-hole-terminating virtual particle-pair trajectories provide regions of excitation beyond the event horizon that can be stimulated to emit photons, with the necessary energy and momentum information conveyed via the virtual pair. These processes are the black hole analogy of the atomic processes depicted in Fig. IV.1, and allow for the possibility that the relevant cross sections can be bigger than the geometric size of the black hole.

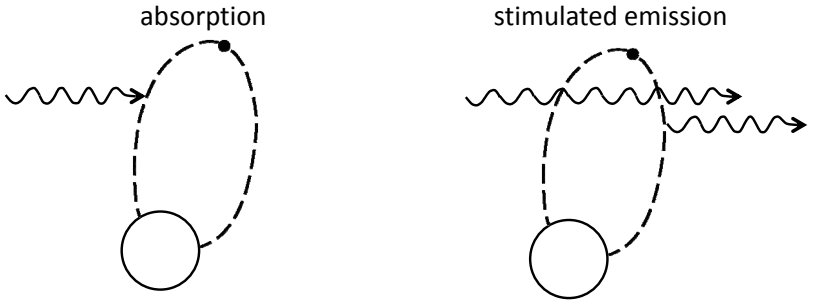

Fig. IV.B.3. Schematic depictions of the absorption of a photon incident on a black hole (left) and the stimulated emission from a black hole induced by an incident photon (right). The large open black circles depict the event horizons. The small-solid circles display the birth locations of virtual electron-positron pairs whose trajectories (dashed curve) terminate on the black holes. See the main text for further discussion.

IV.C Transition state theory of particle emission

In general, the Weiskopf emission theory used in the previous sections has been superseded by more complete methods using transition state theory [EYR35, EVA35, BOH39]. These enable the tracking of the orbital angular momentum of the emitted particles, and the total angular momentum of the emitting system. The central equation in transition state theory is the probability per unit time that a complex system accesses a given configuration (state)

$$P = \frac{1}{h\rho} \ , \qquad \text{(IV.C.1)}$$

where ρ is the total level density of the system. For those not familiar with transition state theory, Eq. (IV.C.1) may appear to be a magical equation not to be trusted. For those familiar with transition state theory, it is the cornerstone. To enable those not familiar with Eq. (IV.C.1) to obtain a better feel for its usefulness and relevance, we will first attempt to justify it via simple theoretical considerations, and then demonstrate that, when applied correctly, it gives the same results as those obtained by other methods. In some cases, transition state theory causes the math to solve a given problem to become more complex (see section IV.C.1), while in other problems which might appear very complex, transition state theory enables a simple solution.

In an oversimplification of reality, Eq. (IV.C.1) can be obtained assuming a system with total energy E has a uniform density of states about this energy of $\rho = 1/\Delta$, with total energies $E_n = E + n\cdot\Delta$ with n being integers. Given that this excited configuration lives for a finite time period, via the time-energy

uncertainty principle the total energy cannot be the precise value E, with the wave-function of the system being a linear combination of wave functions

$$\psi = \sum_n \psi_n \exp(-iE_n t/\hbar) \propto \sum_n \psi_n \exp(-in\Delta \cdot t/\hbar) \qquad \text{(IV.C.2)}$$

The complexity of this wave function depends of the number of n needed to characterize the system. However, this wave function is cyclic, repeating itself every $\tau = h/\Delta = h\rho$. A more detailed analysis where the state density is not uniform gives a more chaotic time dependence, but the time scale for finding a given state is still given by $\tau = h\rho$.

The time evolution of the system can be considered as a series of jumps between configurations (states), with some of these states being doorway or transition states to a non-reversible change. For example, if a hot nucleus (parent system) with total energy E can arrange itself so it looks like a hot nucleus with one less neutron (daughter system) with energy $E-\varepsilon_n-B_n$, with the rest of the energy confined to a single neutron with enough energy to escape from the daughter system, then this configuration will make the non-reversible transition to the daughter plus the emitted neutron. The calculation of the rate of particle emission can thus be transformed into a matter of determining the total level density, ρ, and counting the number of relevant transition states, N_{ts}, and using the equation

$$R = \frac{N_{\text{ts}}}{h\rho} \ . \qquad \text{(IV.C.3)}$$

For those who have not previously used transition state theory, it is possible that you are not yet convinced of its correctness and/or usefulness in the case of particle-emission problems. To dispel any doubts we shall, in the next two subsections, use transition state theory to calculate the emission of massive Bosons from an oven, and calculate the emission of neutrons from a hot nucleus. In section IV.C.3 we will use transition state theory to calculate the photon emission from a black body and obtain the same results as from section IV.B.

IV.C.1 Emission of massive Bosons from an oven

To calculate the emission of a massive Boson (e.g. ^{4}He atoms) through a small hole in an oven at temperature T, containing a large number of identical Bosons using Eq. (IV.C.3), all we need to do is determine the density of states, and the relevant number of transition states. The entropy of an ideal gas with energy U, containing N particles, each of mass m, in a container of volume V can be expressed as

$$S = Nk\frac{3}{2}\ln\left[\frac{mT}{2\pi\hbar^2}\left(\frac{V}{N}\right)^{2/3}\right] = k\ln(\rho)\,, \qquad \text{(IV.C.4)}$$

and thus

$$\rho(U) = \left[\left(\frac{mT}{2\pi\hbar^2}\right)^{3/2}\frac{V}{N}\right]^N \ . \qquad \text{(IV.C.5)}$$

These equations are only valid for an ideal (classical) gas of massive Bosons ($T << mc^2$), which requires the number density n, of the Bosons to be much smaller than $n_c = [mT/(2\pi\hbar^2)]^{3/2}$. Near and above this number density, one must switch from Boltzmann to Bose-Einstein statistics.

For simplicity, we assume a spherical container with a radius r, with a small hole of area σ in the surface of the sphere. The number of transition states for the emission of particles from the oven, through the hole, with kinetic energies between ε and $\varepsilon + d\varepsilon$ is

$$N_{\rm ts} = \sum_{L=0}^{L_{\rm max}} (2L+1) \frac{\sigma}{4\pi r^2} \rho_{\rm f}(U-\varepsilon) d\varepsilon \,. \qquad \text{(IV.C.6)}$$

The factor of $\sigma/(4\pi r^2)$ gives the fraction of a given L state that corresponds to particles on a trajectory that will pass through the hole in the surface, and exit the container. The subscript f denotes the final system after the emission of the particle. For an emitted particle with kinetic energy ε and mass m, the maximum angular momentum squared is given by

$$L_{\rm max}^2 \hbar^2 = \left(mr\sqrt{\frac{2\varepsilon}{m}} \right)^2 = 2m\varepsilon r^2 \,. \qquad \text{(IV.C.7)}$$

Assuming a large classical system with $L_{\rm max} >> 1$, gives the particle emission rate of

$$R(\varepsilon)d\varepsilon = (L_{\rm max}+1)^2 \frac{\sigma}{4\pi r^2} \frac{\rho_{\rm f}(U-\varepsilon)}{h\rho_{\rm i}(U)} d\varepsilon \sim \frac{2m\sigma\varepsilon}{8\pi^2\hbar^3} \frac{\rho_{\rm f}(U-\varepsilon)}{\rho_{\rm i}(U)} d\varepsilon \,. \qquad \text{(IV.C.8)}$$

The subscript i denotes the initial system before the emission of a particle. The total energy of the particles in the oven after the emission of a single particle of energy ε is

$$U-\varepsilon = \frac{3}{2} T_{\rm f}(N-1) = \frac{3}{2} T_{\rm i} N - \varepsilon \,, \quad \text{and thus} \quad T_{\rm f} = T_{\rm i} \frac{N}{(N-1)} - \frac{2}{3} \frac{\varepsilon}{(N-1)} \,. \qquad \text{(IV.C.9)}$$

The ratio of the final to initial state densities of the particles in the oven is then

$$\frac{\rho_{\rm f}(U-\varepsilon)}{\rho_{\rm i}(U)} = \left[\left(\frac{mT_{\rm i}(\frac{N}{N-1} - \frac{2}{3}\frac{\varepsilon}{T_{\rm i}(N-1)})}{2\pi\hbar^2} \right)^{3/2} \frac{V}{N-1} \right]^{N-1} \cdot \left[\left(\frac{mT_{\rm i}}{2\pi\hbar^2} \right)^{3/2} \frac{V}{N} \right]^{-N}$$

$$= \left(\frac{2\pi\hbar^2}{mT_{\rm i}} \right)^{3/2} \frac{1}{V} \frac{N^N}{(N-1)^{N-1}} \left(\frac{N}{N-1} - \frac{2\varepsilon}{3T_{\rm i}(N-1)} \right)^{3(N-1)/2} \,. \qquad \text{(IV.C.10)}$$

In the limit as the number of particles goes to infinity, this ratio becomes

$$\frac{\rho_{\rm f}(U-\varepsilon)}{\rho_{\rm i}(U)} = n \left(\frac{2\pi\hbar^2}{mT_{\rm i}} \right)^{3/2} \left(1 - \frac{2\varepsilon}{3T_{\rm i}(N-1)} \right)^{3(N-1)/2} = n \left(\frac{2\pi\hbar^2}{mT} \right)^{3/2} \exp(-\varepsilon/T) \,, \qquad \text{(IV.C.11)}$$

and thus the emission rate becomes

$$R(\varepsilon)d\varepsilon = \frac{2m\sigma\varepsilon}{8\pi^2\hbar^3} n \left(\frac{2\pi\hbar^2}{mT} \right)^{3/2} \exp(-\varepsilon/T) d\varepsilon = \frac{\sigma n \varepsilon \exp(-\varepsilon/T) d\varepsilon}{T\sqrt{2\pi mT}} \,, \qquad \text{(IV.C.12)}$$

in agreement with other methods [CLE07].

IV.C.2 Neutron emission from hot nuclei

Now that we have some experience using transition state theory, we can proceed at a faster rate. The rate of emission of neutrons (with spin $s = 1/2$) from a spherical hot spinning nucleus with excitation energy E, and angular momentum $J_{\rm i}$, can be expressed as

$$R = \frac{N_{\rm ts}}{h\rho} = \frac{1}{h\rho_{\rm i}(E - E_{\rm rot}(J_{\rm i}))} \int_0^\infty \sum_{L=0}^{\infty} \sum_{J=|L-s|}^{J=|L+s|} \sum_{J_{\rm f}=|J_{\rm i}-J|}^{|J_{\rm i}+J|} T_J(\varepsilon) \rho_{\rm f}(E - E_{\rm rot}(J_{\rm f}) - \varepsilon - B_{\rm n}) d\varepsilon \,, \qquad \text{(IV.C.13)}$$

where $T_J(\varepsilon)$ are the transmission coefficients associated with the absorption of neutrons of kinetic energy ε, and angular momentum J. For each nucleus at a given angular momentum there is a minimum energy

$E_{\rm rot}(J)$ relative to the minimum energy irrespective of spin. The energy above $E_{\rm rot}(J)$ is associated with thermal excitation (heat) and follows statistical rules when this thermal-excitation energy becomes large compared to the spacing between the low-lying quantum levels. We have already cut corners a little by not tracking parity in Eq. (IV.C.13). Adding the assumption of a large system with $J_{\rm i} >> 1$, and the assumption that the modification of the spin associated with the emission does not substantially modify the rotational energy $E_{\rm rot}$ (often justifiable for neutron emission in heavy-ion reactions) gives

$$R \sim \frac{2s+1}{h\rho_{\rm i}(U)} \int_0^\infty \sum_{L=0}^{\infty} (2L+1) T_L(\varepsilon) \rho_{\rm f}(U-\varepsilon-B_{\rm n}) d\varepsilon \,, \qquad \text{(IV.C.14)}$$

where U is the thermal-excitation energy of the initial nucleus. The $T_L(\varepsilon)$ could be assessed using carefully measured absorption cross sections for the reverse process, and its corresponding theoretical representation

$$\sigma_{\rm a}(\varepsilon) = \sum_{L=0}^{\infty} (2L+1) \pi \lambda\!\!\!^{-2} T_L(\varepsilon) \,. \qquad \text{(IV.C.15)}$$

However, in general, the transmission coefficients are calculated using nuclear potential models obtained by an evaluation of particle scattering data. Here, to obtain a nice analytical expression, we further assume the neutron-transmission coefficients behave classically with $T_L(\varepsilon) = 1$ for $L < L_{\rm max}$ (otherwise 0) with $L_{\rm max} = r(2m\varepsilon)^{1/2}/\hbar$, where r is the barrier radius (typically ~1 fm larger than the radius of the final nucleus); and assuming changes in the level density of a hot nucleus (Fermi gas) can be assessed via a simple Boltzmann factor. These assumptions lead to the result

$$R \sim \frac{2s+1}{2\pi\hbar} \int_0^\infty L_{\rm max}^2 \exp(-\varepsilon/T) d\varepsilon \exp(-B_{\rm n}/T) = \frac{2s+1}{2\pi\hbar} \frac{2mr^2}{\hbar^2} \int_0^\infty \varepsilon \exp(-\varepsilon/T) d\varepsilon \exp(-B_{\rm n}/T)$$

$$\sim \frac{(2s+1)\sigma_{\rm a} m T^2}{\pi^2 \hbar^3} \exp(-B_{\rm n}/T), \qquad \text{(IV.C.16)}$$

in agreement with Eq. (IV.A.3) obtained via the Weisskopf method. The simplifications following Eq. (IV.C.14) are only used here to demonstrate the conditions under which the method in this subsection is equivalent with the Weisskopf method discussed earlier, and are not (in general) used in modern nuclear-reaction theory codes.

IV.C.3 Semi-classical black-body emission

Following the same logic used for neutron emission in section IV.C.2, we write the transition state theory emission rate of uncorrelated photons from a large black-body sphere as

$$R = \frac{2}{2\pi\hbar} \int_0^\infty \sum_{L=0}^{L_{\rm max}} (2L+1) \exp(-\varepsilon/T) d\varepsilon \,. \qquad \text{(IV.C.17)}$$

Notice that the factor of $2s+1$ for a massive particle is here replaced by 2 for the two states of photon helicity (or two states of polarization). The maximum angular momentum that a photon can carry away from a macroscopic sphere of radius r is $L_{\rm max}\hbar = r\varepsilon/c$. Substitution into Eq. (IV.C.17) gives

$$R = \frac{4\pi r^2}{4\pi^2 \hbar^3 c^2} \int_0^\infty \varepsilon^2 \exp(-\varepsilon/T) d\varepsilon \,, \qquad \text{(IV.C.18)}$$

in agreement with the uncorrelated spontaneous single-photon emission rate obtained in section IV.B. In section IV.B we justified the replacement of the classical exponential term with the corresponding

Planckian factor using the ratio of stimulated to spontaneous emission obtained by Einstein [EIN17]. This replacement of the simple exponential with the Planckian factor can also be justified by the semi-classical addition of stimulated emission in the surface of black bodies [LES08b]. This derivation is long and detailed, and presented in Appendix A for the fastidious reader. The main results from Appendix A are: Eq. (IV.C.18) is the rate of photon emission from events consisting of a single uncorrelated photon; and the photon-emission rate associated with events containing a multiplicity of n correlated photons is $f^{n-1} \times$ Eq. (IV.C.18), where $f = \exp(-\varepsilon/T)$. It then follows that the ratio of correlated to uncorrelated photons is given by $f + f^2 + f^3 + \ldots = [\exp(\varepsilon/T) - 1]^{-1}$ and thus the total photon-emission rate can be obtained by replacing the exponential factor in Eq. (IV.C.18) with the corresponding Planckian factor, as previously discussed.

One can go further and show that Poissonianly distributed spontaneous emission in the surface of a black body, with the semi-classical inclusion of stimulated emission [LES08b] leads to photon counting statistics as given by a negative binomial distribution [BEE99, CLE07] in agreement with quantum theory and consistent with the entropy fluctuation theorem [CLE07], and also leads to a semi-classical understanding of the Hanbury Brown and Twiss effect for black bodies (see Appendix B).

IV.D Hanbury Brown and Twiss effect by semi-classical means

The Hanbury Brown and Twiss effect [HAN56] is one of the cornerstones of quantum optics. It is the process by which optical photon-photon correlations discussed in the previous section are seen at a distance from an object of interest. It can be used to infer the shape and size of distant objects that otherwise appear to be point-like, and is the optical analogy of radio-astronomy techniques that use the correlation of radio-signals across arrays of spatially separated telescopes to infer details not observable by a single radio telescope. One of the first practical uses of the Hanbury Brown and Twiss effect was to measure the angular size of stars, and thus confirm astrophysical calculations of their size. This topic is therefore often taught in undergraduate astronomy classes.

From classical electromagnetic (wave) theory one can show that the cross correlation between two separated intensity detectors in given by [PUR56]

$$< S_1 S_2 >= \overline{S}_1 \overline{S}_2 \left(1 + \frac{\tau}{dt} F(r_1, r_2) \right), \tag{IV.D.1}$$

where S_1 and S_2 are the time dependent signals in detectors 1 and 2, τ is the coherence time given by the inverse of the width of the frequency response of the system, dt is the time resolution, and $F(r_1,r_2)$ is the diffraction pattern associated with an aperture equal to the cross-section of the source as viewed from the detector locations. Properties of the $F(r_1,r_2)$ include [BOR95] $F(r_1,r_1) = 1$; $F(r_1,r_2) = 0$ if the two detectors are separated by a distance much larger than the wavelength divided by the angular size of the source; and

$$\iint_{r_2(\theta,\phi)} \frac{\sigma}{\lambda^2} F(r_1, r_2) d\Omega = 1 . \tag{IV.D.2}$$

Hanbury Brown and Twiss [HAN56] made the bold assumption, for that time, that Eq. (IV.D.1) would still be valid for optical measurements where the detectors were counting individual photons and not the intensity of the incoming waves as done in radio astronomy.

The history of the confirmation of the Hanbury Brown and Twiss effect is fascinating, with many years between its original discovery and the wide acceptance of the reality of this phenomenon. Initially, many physicists refused to believe the original observations. This was not helped by other authors who tried to repeat the original study, but failed to see the photon correlations because of inadequacies in

their experimental setups. The paradigm shift to acceptance was facilitated by QED calculations [FAN61] that placed the reason for the experimental observation on a strong theoretical footing. The essence of this explanation is partially depicted in Fig. IV.D.1 showing two source locations A and B separated by a distance r, and two detector locations 1 and 2 separated by x, with both of these separations perpendicular to the vector of length d, characterizing the separation of the observer from the light source(s). In quantum theory, the probability of an event is first characterized by an amplitude A, which is squared to obtain the event probability. Given the assumption that d is very much larger than both r and x, and identical sources and detectors, the amplitude for a photon transition from A→1, A→2, B→1, and B→2 are equal and here denoted by the value A. There are two ways of seeing two detections at the same time. These are: one photon travels from A to 1 with the other travelling from B to 2; and one photon going from A to 2 with the other passing from B to 1. Thinking classically, these two ways of seeing a simultaneous detection are distinguishable, and the probability of seeing two photons at the same time in detectors 1 and 2 can be written

$$\mathrm{P_C} = \left|A_{\mathrm{A}\to 1,\mathrm{B}\to 2}\right|^2 + \left|A_{\mathrm{A}\to 2,\mathrm{B}\to 1}\right|^2 = \left|A_{\mathrm{A}\to 1}\times A_{\mathrm{B}\to 2}\right|^2 + \left|A_{\mathrm{A}\to 2}\times A_{\mathrm{B}\to 1}\right|^2 = \left|A^2\right|^2 + \left|A^2\right|^2 = 2A^4 . \qquad \text{(IV.D.3)}$$

To put it more succinctly, if the probability of a single photon going from the source to a detector is $\mathrm{P}=A^2$, then the probability of simultaneous detections in the two detectors is proportional to $2\mathrm{P}^2$, i.e. $2A^4$. The factor of two is associated with the two distinct ways of bringing about a simultaneous detection. However, quantum theory introduces some subtle effects. If the two ways of seeing simultaneous detections are distinguishable by the observer then Eq. (IV.D.3) applies. However, if the two ways of seeing the event are indistinguishable then the rules of quantum theory state the amplitude for the two indistinguishable ways must be added (for Bosons) before squaring. This is analogous to the double-slit scattering experiment where, if the observer cannot tell which slit a photon goes through, the amplitudes for each possible path are added before squaring. Therefore, if the two ways of seeing simultaneous detections are not distinguishable then the probability of this type of event is given by

$$\mathrm{P}^* = \left|A_{\mathrm{A}\to 1,\mathrm{B}\to 2} + A_{\mathrm{A}\to 2,\mathrm{B}\to 1}\right|^2 = \left|A^2 + A^2\right|^2 = 4A^4 = 2\mathrm{P_C}\,, \qquad \text{(IV.D.4)}$$

twice the classical result. Now we need to determine when the two ways of seeing a simultaneous detection are indistinguishable.

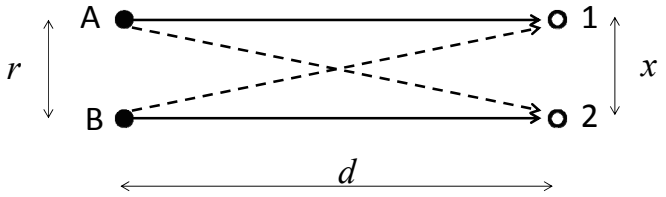

Fig. IV.D.1. Schematic depiction of two source locations, A and B, two photon detector locations, 1 and 2, and the two ways of observing a simultaneous detection in both detectors (solid and dashed lines).

To proceed, we assume the source(s) emit photons of energy ε, and thus have momenta of $p=\varepsilon/c$, and a reduced wavelength of $\lambda\!\!\!^{-} = \hbar/p$. However, if the object has a size r in the vertical direction (see Fig. IV.D.1) then, via the uncertainty principle, the photons must have an uncertainty in their momentum in this direction of $\Delta p \sim \hbar/r$. This means that, when detected, there is no way the observer can assign the incoming angle of the photons to better than $\Delta\theta \sim \Delta p/p \sim \lambda\!\!\!^{-}/r$. The angular separation of the detectors as viewed by a given source location is $\Delta\phi = x/d$. This is the change in angle required to switch a photon's trajectory from going from detector 1 to detector 2, or vice-versa. If this angular change is very much smaller than the limit of our knowledge of the photon's direction as defined by the uncertainty principle,

i.e. $\Delta\phi << \Delta\theta$, then it is not possible to distinguish between the two ways of defining a simultaneous detection, and Eq. (IV.D.4) applies. Similarly if $\Delta\phi >> \Delta\theta$, then Eq. (IV.D.3) applies. The transition between these limits is at $\Delta\phi \sim \Delta\theta$, and thus at $x \sim \lambda\!\!\!^{-}/\theta$, where $\theta = r/d$ is the angular size of the object.

As an example of the implications of the above discussed theory, consider the star Sirius A first observed by Hanbury Brown and Twiss (in 1956) with a radius of 1.2 million km at a distance of 8.6 light-years and thus an angular size of 1.5×10^{-8} rad. If viewed by idealized detectors observing blue-green light with a wave length of ~450 nm ($\lambda\!\!\!^{-} = 7.2\times10^{-8}$ m), then the characteristic length scale between a detector pair for the transition from Eq. (IV.D.4) to Eq. (IV.D.3) is ~5 m. According to the simplistic arguments discussed in the last few paragraphs, the coincidence rate with a pair of detectors separated by $x << 5$ m, should be twice the classical rate observed with $x >> 5$ m. However, this is the theoretical limit of the transition, and applies only to idealized detectors. You may have noticed that we have not discussed the complexities of what it means for a pair of photons to be simultaneously observed in a pair of spatially separated detectors. These complexities can significantly reduce the size of the transition from a factor of 2 to values close to unity. This is, in part, why some experimentalists did not at first confirm the initial results of Hanbury Brown and Twiss.

Unfortunately, attempts to translate the QED picture of the Hanbury Brown and Twiss effect into semi-classical arguments, to enable the teaching of undergraduate astronomy students, has led to a misunderstanding of the true nature of the phenomenon by a generation of astronomy students from some institutions. I have several colleagues who have been taught the incorrect semi-classical argument that the Hanbury Brown and Twiss effect is caused by long-range photon-photon interactions as they travel through free space that cause independent and widely-spaced emissions from a star to become correlated and thus arrive "together" in time at detectors separated by less than $x \sim \lambda\!\!\!^{-}/\theta$.

IV.D.1 Simple two-atom system

Instead of embarking on a semi-classical explanation of the Hanbury Brown and Twiss effect for a large black-body object, we here consider the simpler case of a two-excited-atom system in a cylindrical container as depicted in Fig. IV.D.2. The more complex problem of a black body is addressed in Appendix B. We start by determining the emission rate for photons from a two-state atom with excitation energy ε. This can be done by assuming the spontaneous emission is, in fact, a stimulated emission where the inducing photon is a virtual-vacuum photon. We assume the photon absorption cross section for making the transition from the ground state to the excited state is σ_a if the energy of the photon is within $d\varepsilon/2$ of the mean transition energy ε. As discussed earlier, the stimulated-emission cross section is the same as the absorption cross section. We have previously determined that the number density of photon states is given by $n(\varepsilon)d\varepsilon = \varepsilon^2 d\varepsilon/(\pi^2\hbar^3c^3)$ [see Eq. (IV.B.4)]. Each of these states is occupied by a virtual-vacuum photon. The rate of spontaneous emission from an excited state can be determined by considering the fraction of virtual photons in a spherical shell of radius r and thickness dr surrounding an excited atom that will interact with it. This fraction is $\sigma_a/(4\pi r^2)$. The rate of spontaneous emission is the number of virtual photons in the above-discussed shell multiplied by the fraction that interact, divided by the time it takes the interacting photons to clear the shell, and is given by

$$R(\varepsilon) = \frac{\varepsilon^2 d\varepsilon 4\pi r^2 dr}{\pi^2\hbar^3c^3}\frac{\sigma_a}{4\pi r^2}\frac{c}{dr} = \frac{\varepsilon^2\sigma_a d\varepsilon}{\pi^2\hbar^3c^2} \qquad \text{(IV.D.5)}$$

We assume the two detectors have identical angular sizes $d\Omega$, and identical polarization filters that transmit only one of the two possible states of polarization. The probability for observing a photon in

detector 1 emitted from atom A in the time interval dt is $P_{A\to1}= R/2\cdot dt\cdot d\Omega/(4\pi)$. R is divided by two because we here assume only one of the polarization states in observed. The probability of an accidental coincidence within a time window of dt is thus given by

$$P_A = P_{A\to1}P_{B\to2} + P_{A\to2}P_{B\to1} = 2\left(\frac{R}{2}\frac{d\Omega}{4\pi}dt\right)^2. \tag{IV.D.6}$$

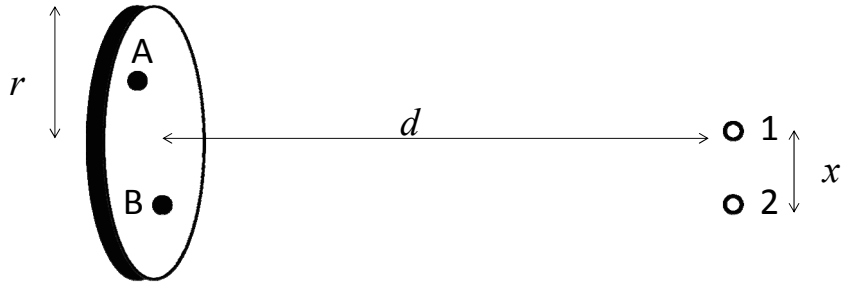

Fig. IV.D.2. Atoms A and B in a cylindrical container observed by the two detectors 1 and 2.

At any point in time we can label one of the atoms as being the back atom (the one closest to the back of the cylinder as viewed from the detector pair). The probability per unit time that the back atom emits a photon that is detected by either of the detectors is $2[R/2\cdot dt\cdot d\Omega/(4\pi)]= R\cdot dt\cdot d\Omega/(4\pi)$. The probability that this emission stimulates the forward atom to emit its photon is given by σ_a/σ_c, where σ_c is the cross-sectional area of the cylinder. Given the second photon is generated by stimulated emission, one might, at first think that the two photons are heading in the same direction. This would only be the case in the limit of an infinite cylinder radius. For a finite cylinder radius, the first detected photon defines the diffraction axis. The second photon is diffracted relative to this axis with a probability of being seen in the other detector given by $\sigma_c\cdot F(r_1,r_2)d\Omega/\lambda^2$ [see Eq. (IV.D.2)]. The probability of seeing a real coincidence is therefore given by

$$\begin{aligned} P_R &= R\frac{d\Omega}{4\pi}dt\frac{\sigma_a}{\sigma_c}\frac{\sigma_c}{\lambda^2}F(r_1,r_2)d\Omega = 4\left(\frac{R}{2}\frac{d\Omega dt}{4\pi}\right)^2\frac{4\pi}{Rdt}\frac{\sigma_a}{\lambda^2}F(r_1,r_2) \\ &= 2P_A\frac{\pi^2\hbar^3c^2 4\pi}{\varepsilon^2\sigma_a d\varepsilon dt}\frac{\sigma_a}{\lambda^2}F(r_1,r_2) = P_A\frac{1}{d\nu dt}F(r_1,r_2) = P_A\frac{\tau}{dt}F(r_1,r_2). \end{aligned} \tag{IV.D.7}$$

The probability of seeing either coincidence type is

$$P_{coincidence} = P_A\left(1+\frac{\tau}{dt}F(r_1,r_2)\right). \tag{IV.D.8}$$

Here we have not considered the time difference between the two real coincidence events associated with the time-energy uncertainties principle, and have thus assumed $dt >> \tau$. Including this effect, in the limit of idealized (perfect) detectors operating at quantum limits, gives $dt = \tau$, and the simplified result discussed earlier, where for detectors separated by a distance $<< \lambda/\theta$, the coincidence rate is twice the classical expectation.

Eq. (IV.D.8) applies for two detectors with identical polarization filters. This is not the standard method of defining the Hanbury Brown and Twiss effect. Instead, the standard is with the cross-correlation signal (the product of both intensities) with detectors observing both polarization states. To obtain the cross-correlation signal for optical photon counting, we assume the detection of each photon generates a unit current for a time period dt after the initial detection. The product of the signals from both detectors is thus one unit for the time period that the signals from both detectors are overlapping. The removal of the polarization filters doubles the rate of photon detection in both detectors. The

accidental coincidence rate is therefore quadrupled. However, the length of the cross-correlation current varies from dt for perfectly overlapping accidental coincidences to near zero for those separated in time by nearly dt, and thus barely overlapping. The average cross-correlation signal length per accidental coincidence is therefore $dt/2$. For real coincidences without polarization filters the probability of the first detection goes up by a factor of two. In the case of the cross-correlation signal for real coincidences, as long as $dt >> \tau$, the coincidences are all perfectly overlapping, and always give the full signal current for the time period dt. Notice that the switch to the cross-correlation signals with no polarization filters changes the accidental coincidence signal by a factor of $4\times1/2=2$, while the real coincidence signal is modified by a factor of 2. These factors being the same means that the Hanbury Brown and Twiss effect is the same for coincidence rates with a pair of identical detectors each seeing only one state of polarization, or for the cross-correlation signal between a pair of detectors seeing both states of polarization. The corresponding Hanbury Brown and Twiss effect is obtained for black bodies by semi-classical means in Appendix B.

V. Photon emission from a black hole

Before we calculate the force associated with the exchange of photons between a pair of black holes, we must become familiar with the emission and absorption properties of a single isolated black hole. As discussed previously, the emission from hot (i.e. thermodynamic) objects can often be studied by considering the absorption process. This means that, after it was determined that black holes are thermodynamic objects with a temperature of [HAW74]

$$T = \frac{\hbar c}{4\pi r_S} = \frac{E_{RP}^2}{mc^2}, \tag{V.1}$$

where r_S is the Schwarzschild radius, m is the black hole's mass, and $E_{RP} = [\hbar c^5/(8\pi G)]^{1/2} = 3.9\times10^8$ J is the reduced Planck energy, then the photon emission can be determined by studying the much simpler photon absorption process. In the limit that the photon wavelength is much smaller than the size of the black hole, the paths and thus the absorption cross section can be determined using geometric optics (i.e ignoring the wave-like nature of light). However, if the reduced wavelengths of the incident photons (at infinity) are comparable to or larger than r_S then wave optics is needed.

V.A Geometric optics

Any good introductory general relativity text book gives the equations of motion of a photon incident on a Schwarzschild black hole with an impact parameter b

$$\left(\frac{dr}{dt}\right)^2 = \left(1 - \frac{b^2(1-1/r)}{r^2}\right)(1-1/r)^2 \quad \text{and} \quad \frac{d\theta}{dt} = \frac{b}{r^2}(1-1/r). \tag{V.A.1}$$

Here, the lengths are in units of r_S. Photon paths for various impact parameters are displayed in Fig. V.A.1. For non-captured photons, the path of closest approach r_c can be obtained by setting the derivative of the distance from the black hole with respect to time equal to zero. This leads to the expressions

$$b^2 = \frac{r_c^3}{r_c - 1} \quad \text{and thus} \quad \frac{db^2}{dr_c} = \frac{3r_c^2}{r_c - 1} - \frac{r_c^3}{(r_c-1)^2} \quad . \tag{V.A.2}$$

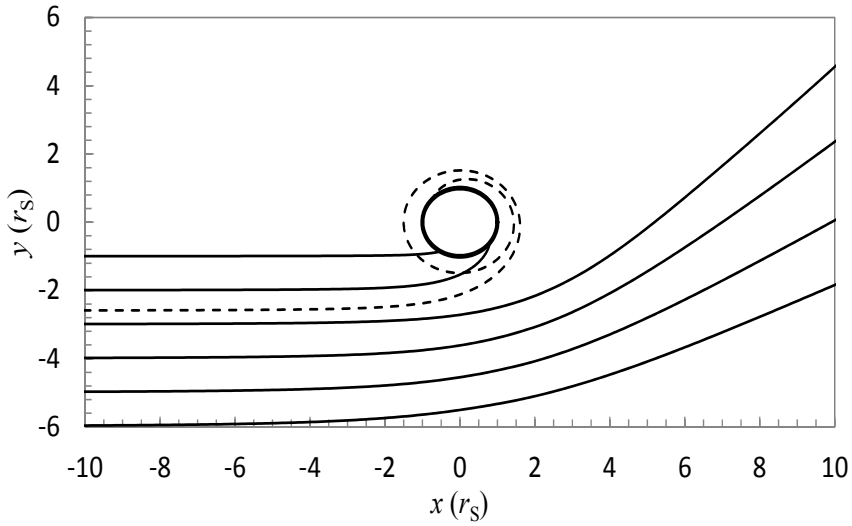

Fig. V.A.1. Various photon paths in the presence of a Schwarzschild black hole. The thick-black circle shows the event horizon. The black curves display paths with impact parameters of r_S to $6r_S$ in steps of r_S. The dashed curve shows a path with an impact parameter just inside the transition from non-capture to capture paths.

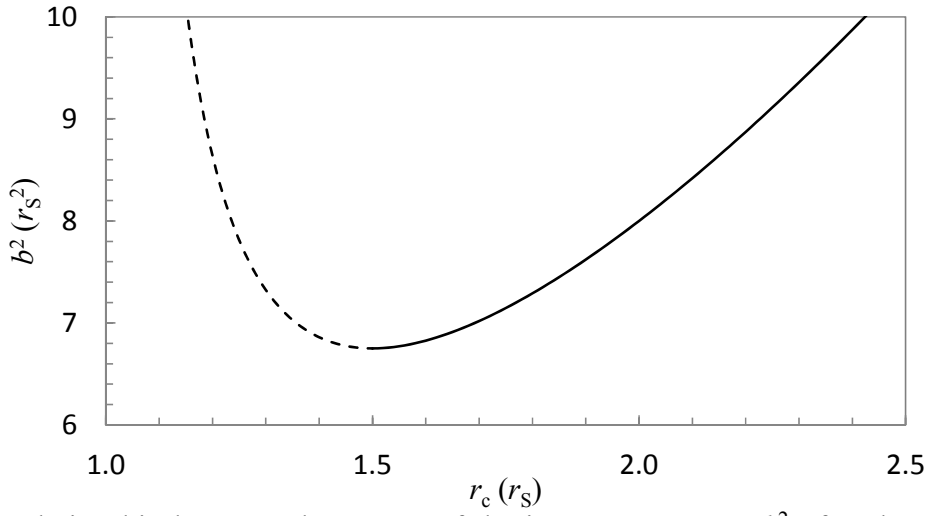

Fig. V.A.2. The relationship between the square of the impact parameter b^2 of a photon incident on a Schwarzschild black hole on the distance of closest approach r_c. The turning point is at $r_c = 3/2$ and $b^2 = 27/4$, and marks the transition between non-capture and capture paths. The solid curve shows the physical solutions with a positive slope. The dashed curve shows the unphysical solutions.

For "real" physical non-capture paths, the derivative of b^2 with respect to r_c must be positive. This is only true for solutions to Eq. (V.A.2) with r_c larger than the location of the minimum in b^2 as a function of r_c (see Fig. V.A.2). This minimum at $r_c = 3/2$ marks the transition between non-capture and capture paths, and gives the absorption cross section of $\sigma_a = \pi b^2 = 27\pi/4$. The independence of the capture cross section on photon energy means that if geometric optics is valid then the emission properties will be as those discussed in section IV.B and the emission spectrum would be Planckian as given by Eq. (IV.B.7). However, if this were true then the emitted photons would have energies of $\sim T$ and thus reduced wavelengths of $\sim \hbar c/T \sim 4\pi r_S$. Incident photons with reduced wavelengths larger than the size of the

black hole invalidate the assumption of geometric optics, and thus we must switch to a wave optics formulism to obtain an accurate description of the emission properties.

V.B Wave optics

The emission and absorption of photons by a Schwarzschild black hole are controlled by an energy and angular momentum dependent absorption cross section [FAB75, CRI07]

$$\sigma_{\mathrm{a}}(M\omega) = \sum_{L=1}^{\infty} \frac{(2L+1)\pi r_S^2}{4(M\omega)^2} T_L(M\omega)\,, \tag{V.B.1}$$

where the $T_L(M\omega)$ are transmission coefficients, which depend on both the angular momentum quantum number L, and the angular frequency of the photon ω. Crispino et al [CRI07] have calculated the partial absorption cross section of arbitrary frequency photons for a Schwarzschild black hole of mass M, by numerical means. The photon transmission coefficients are obtained by mapping the radial coordinate to the Wheeler coordinate $x = r + 2M \ln[r/(2M)-1]$, and solving the wave equation

$$(\omega^2 - V)[r\varphi_{\omega l}(x)] + \frac{d^2}{dx^2}[r\varphi_{\omega l}(x)] = 0 \tag{V.B.2}$$

using an effective potential

$$V = (\frac{1-2M}{r})\frac{L(L+1)}{r^2}\,. \tag{V.B.3}$$

The partial cross sections, $\sigma_{\mathrm{a}}(L)$, peak at $M\omega \sim (2L+1)/10$ (in units with $c = G = 1$). This behavior is easily understood given the effective potential [Eq. (V.B.3)]. We have independently confirmed the results of Crispino et al by solving Eq. (V.B.2) using the effective potential given by Eq. (V.B.3). Our results are in agreement with the results displayed in figures 1 and 2 of Crispino et al [CRI07]. We have found that an excellent fit to our calculated partial photon-absorption cross sections can be obtained with the function

$$T_L(\omega) = \frac{1}{1 + \dfrac{\exp[(A_L - M\omega)/\delta_L]}{(M\omega)^4}}\,. \tag{V.B.4}$$

The fitting parameters A_L and δ_L are listed in Table V.B.1. Fig. V.B.1 shows the corresponding Schwarzschild photon cross sections obtained using Eq.s (V.B.1) and (V.B.4). These results can be compared directly to the results of Crispino et al [CRI07].

Table V.B.1. The $T_L(\omega)$ fitting parameters, A_L and δ_L for L=1 to 5.

L	1	2	3	4	5
$A_L(M\omega)$	−0.0802	0.3288	0.5990	0.8343	1.0546
$\delta_L(M\omega)$	0.0602	0.0418	0.0367	0.0353	0.0348

Fig. V.B.2 compares the luminosity of a Schwarzschild black hole calculated assuming the absorption cross section is equal to the geometric optics value of $27\pi r_s^2/4$, and assuming the results displayed by the solid curve in Fig. V.B.1, both using Eq. IV.B.7 for the luminosity as a function of photon energy. These calculations compare well with the results of Page [PAG76]. Crispino et al's $M\omega$ can be converted into photon energy relative to the black hole's temperature by multiplying by 8π, i.e. $\varepsilon/T_{\mathrm{bh}} = 8\pi M\omega$.

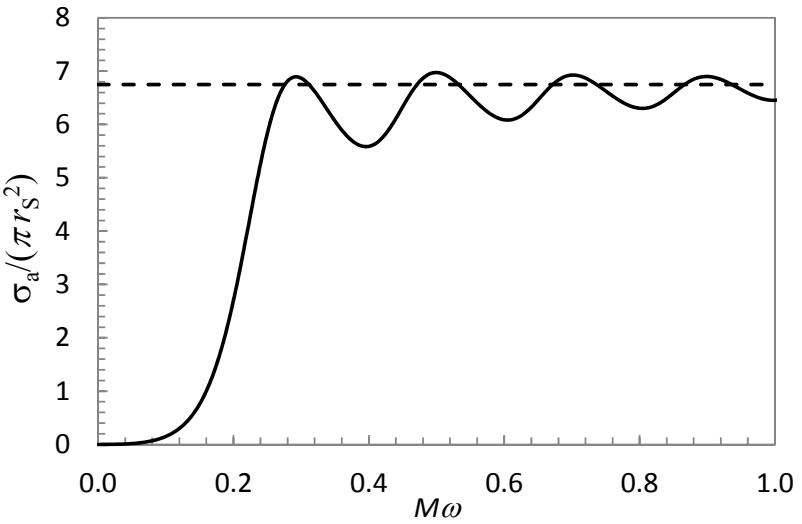

Fig. V.B.1. The black hole photon-absorption cross section as a function of $M\omega$ (solid curve). The dashed line displays the corresponding results using geometric optics.

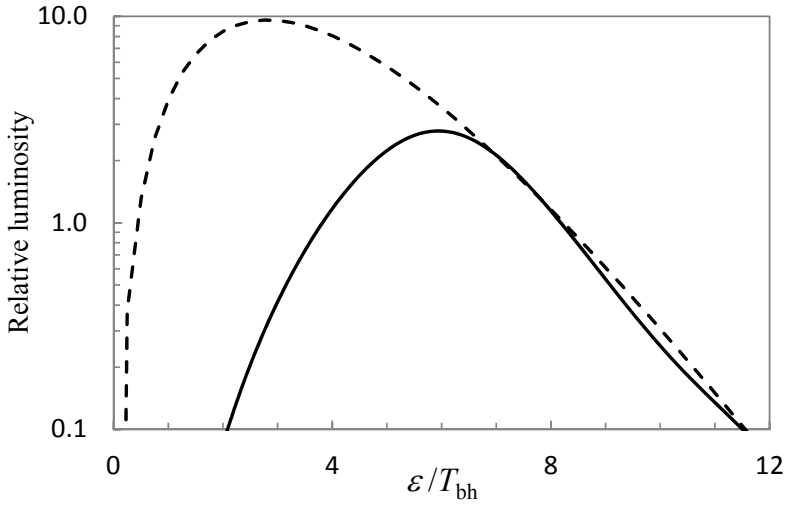

Fig. V.B.2. Luminosity of a black hole calculated using the absorption cross sections displayed in Fig. V.B.1 (solid curve) relative to that obtained using geometric optics (dashed curve).

VI. Classical exchange of photons between a pair of identical objects

Before embarking on a study of photon exchanges between black hole pairs, it is prudent to first consider the exchange of photons between ordinary objects. Material objects at non-zero temperature can both emit and absorb photons, and thus a pair of objects can exchange photons, generating a repulsive force between them. For macroscopic objects this force is, in general, much smaller than the attractive gravitational force between them. However, the exchange of thermal photons between a pair of identical non-charged objects can be used to define an effective charge for the object in question. The power emitted by a spherical black body A and absorbed by an identical object B with radius r, at a distance d, is given by [see Eq. (IV.B.8)]

$$P_{AB} = 4\pi r^2 \frac{\pi^2 T^4}{60c^2\hbar^3}\frac{\pi r^2}{4\pi d^2} = \frac{\pi^3 T^4 r^4}{60\hbar^3 c^2 d^2} \tag{VI.1}$$

with the corresponding repulsive forces associated with the photon exchange being

$$F = \frac{2P_{AB}}{c} = \frac{\pi^3 T^4 r^4}{30\hbar^3 c^3 d^2} = \frac{q_{\text{eff}}^2}{4\pi\varepsilon_0 d^2}. \tag{VI.2}$$

The factor of two is for the two-way exchange. In defining the effective charge q_{eff} of a non-charged black-body sphere, we here ignore the photon emission to infinity, and only consider the photons that are both emitted and absorbed by a pair of identical objects. The corresponding effective charge is given by

$$q_{\text{eff}} = \frac{(\pi T r)^2}{\hbar c}\sqrt{\frac{2\varepsilon_0}{15\hbar c}} = 3.64\times10^{-13}\,\frac{\text{C}}{\text{K}^2 m^2}(Tr)^2. \tag{VI.3}$$

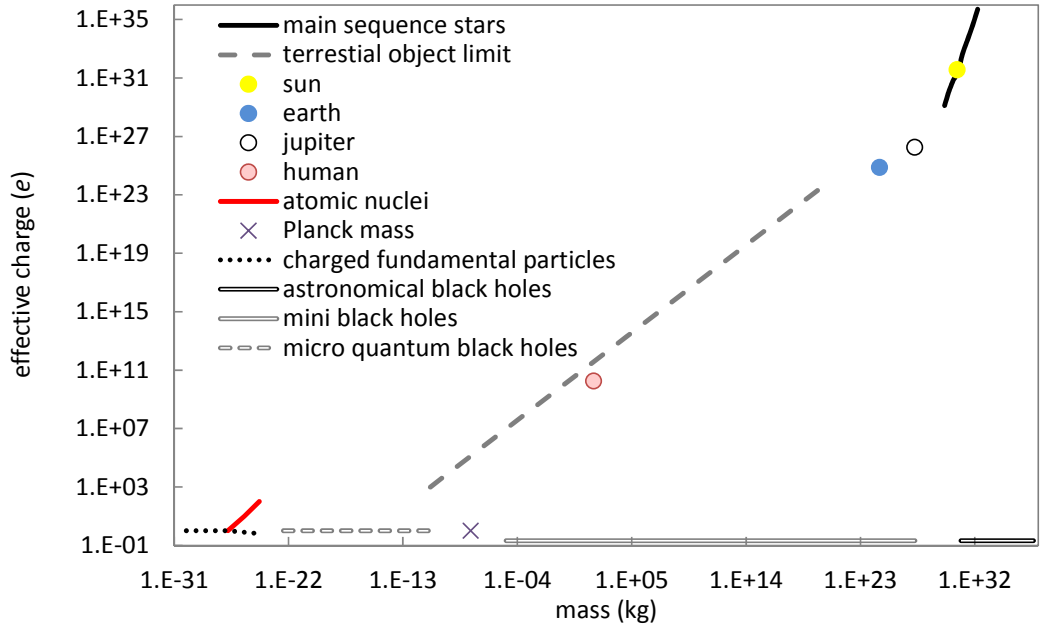

Fig. VI.1. Effective charges, as defined by Eq. (VI.3), of various object types as a function of mass. The dashed-gray line displays the limit for terrestrial objects defined assuming a maximum temperature of ~3000°K and a density of ~10 g/cc, with sizes ranging from large asteroids (r ~100 km) to dust grains (r ~5 μm). Terrestrial objects live below the displayed limit. The Planck mass is displayed with a charge of e by the ×. The displayed charges for the fundamental particles are the real charges of the electron, proton, and top quark (dotted-black line). Likewise the displayed charges of the atomic nuclei are the real charges (solid-red line).

For example, consider to two humans floating in space. We shall here approximate each human as a 100 kg spherical black body at a temperature of 37°C (~310°K) with a density of 1 g/cc, and thus with radii of 28.8 cm. The corresponding effective charge for a human is q_{eff} ~2.9×10^{-9} C. Fig. VI.1 shows the effective charge of various objects in units of the charge on an electron e, versus the object's mass. The dashed line displays the limit for terrestrial objects assuming a maximum temperature of ~3000°K. Above this temperature, objects are assumed to boil away into space, and thus do not exist as a single entity. Notice that only the fundamental particles (and black holes discussed later) have a charge versus mass slope in log-log space of approximately zero. The other objects all significantly increase their

effective charge with increasing mass. The corresponding slopes in log-log space are approximately 2/3, 4/5, and 5/2 for terrestrial objects, atomic nuclei, and main sequence stars, respectively.

VI.A Classical exchange of photons between identical large black holes

In order to obtain a simple analytical expression for the effective charge of large Schwarzschild black holes, we will at first assume that geometric optics apply. In this simplified case the effective charge of a black hole can be obtained via Eq. (VI.3)

$$q_{\text{eff}} = \frac{(\pi T r)^2}{\hbar c}\sqrt{\frac{2\varepsilon_0}{15\hbar c}} = \frac{\pi^2(\hbar c)^2}{\hbar c(4\pi r_{\text{S}})^2}\frac{27 r_S^2}{4}\sqrt{\frac{2\varepsilon_0}{15\hbar c}} = \frac{27}{32}\sqrt{\frac{\varepsilon_0 \hbar c}{30}}. \quad \text{(VI.A.1)}$$

The corresponding effective charge is 0.815×10^{-19} C = $0.509e$ [LES07]. The closeness of this value to the known fundamental unit of charge suggests a possible connection between the existence of this charge and the exchange of photons between black holes.

Switching to wave optics (see section V.B), we must start back at Eq. (IV.B.8) and include the photon energy dependent absorption cross section inside the integral. The corresponding repulsive force associated with the exchange of photons is given by

$$\begin{aligned} F &= \frac{2}{\pi^2 c^3 \hbar^3}\int_0^\infty \frac{\sigma_a(\varepsilon)\varepsilon^3}{[\exp(\varepsilon/T)-1]}\frac{\sigma_a(\varepsilon)}{4\pi d^2}d\varepsilon = \frac{T^4\sigma_a^2(\infty)}{2\pi^3\hbar^3c^3d^2}\frac{\pi^4}{15}\int_0^\infty \frac{15}{\pi^4}\frac{\sigma_a^2(\varepsilon)}{\sigma_a^2(\infty)}\frac{\varepsilon^3 d\varepsilon}{[\exp(\varepsilon)-1]} \\ &= \frac{T^4}{2\pi^3\hbar^3c^3d^2}\left(\frac{27\pi r_{\text{S}}^2}{4}\right)^2\frac{\pi^4}{15}\int_0^\infty \frac{15}{\pi^4}\frac{\sigma_a^2(\varepsilon)}{\sigma_a^2(\infty)}\frac{\varepsilon^3 d\varepsilon}{[\exp(\varepsilon)-1]} = \frac{\pi^3 T^4 r_{\text{S}}^4}{30\hbar^3c^3d^2}\left(\frac{27}{4}\right)^2\int_0^\infty \frac{15}{\pi^4}\frac{\sigma_a^2(\varepsilon)}{\sigma_a^2(\infty)}\frac{\varepsilon^3 d\varepsilon}{[\exp(\varepsilon)-1]}. \end{aligned} \quad \text{(VI.A.2)}$$

The corresponding effective charge is

$$q_{\text{eff}} = \frac{27\pi^2 T^2 r_{\text{S}}^2}{2}\sqrt{\frac{\varepsilon_0}{30\hbar^3c^3}\int_0^\infty \frac{15}{\pi^4}\frac{\sigma_a^2(\varepsilon)}{\sigma_a^2(\infty)}\frac{\varepsilon^3 d\varepsilon}{[\exp(\varepsilon)-1]}} = \frac{27}{32}\sqrt{\frac{\varepsilon_0\hbar c}{30}\int_0^\infty \frac{15}{\pi^4}\frac{\sigma_a^2(\varepsilon)}{\sigma_a^2(\infty)}\frac{\varepsilon^3 d\varepsilon}{[\exp(\varepsilon)-1]}}. \quad \text{(VI.A.3)}$$

Notice that for geometric optics, where the absorption cross section is independent of energy, Eq. (VI.A.3) becomes (VI.A.1). Using the energy-dependent cross section displayed in Fig. V.B.1, the effective charge of black holes, including the wave nature of electromagnetic radiation, is ~0.2e. Astronomical black holes from 2 to 10^6 solar masses are displayed with this effective charge in Fig. VI.1. Mini black holes that may have been formed during the big bang, with a possibility of radiating away during the life time of the universe, are also shown in Fig. VI.1. The corresponding charge-versus-mass slope is zero, and suggests black holes are in the same class of objects as the fundamental particles. We speculate that micro black holes with masses less than the Planck mass, with charges of ~e (see Fig. VI.1), were formed during the very early stages of the big bang and then rapidly evaporated down to the known fundamental particles.

VII. Quantum exchange of photons between a pair of micro black-hole-like objects

Once we consider micro black holes with masses less than the Planck mass, we are necessarily heading into the world of speculation because no unification of quantum mechanics and general relativity exists. By definition, the size of a Planck-mass [$(\hbar c/G)^{1/2}$=2.17647×10^{-8} kg] black hole (assumed to be $2r$s) is the Planck length [$(\hbar G/c^3)^{1/2}$=1.61623×10^{-35} m]. The Planck mass is approximately that of a flea egg, and by itself does not create any theoretical difficulties. However, the Planck length is incredibly small being ~17 orders of magnitude less than the smallest length scale probed in accelerator experiments, and is the length scale below which our theoretical understanding of

space breaks down. Therefore, it is possible that all general-relativity length scales involving Schwarzschild-black-hole event horizons are lost and/or meaningless for micro black holes, with the only remaining measurable properties being mass, and perhaps temperature. Interactions on length scales smaller than the Planck length are likely meaningless. We speculate that in addition to mass and temperature an additional property survives in the sub-Planck mass range. The emission (and absorption) of L=0 photons from black holes is non-physical [CRI07]. However, we speculate that virtual L=0 photons can be exchanged between two micro black holes, and that the relevant transmission coefficient for widely spaced black holes is $T_{L=0}$=1, with a corresponding cross section $\sigma_a = \pi\lambda\!\!\!^{-2}$. This is analogous to the case of neutron absorption by atomic nuclei with a cross section as given in Eq. (IV.C.15). When the neutron wave length is much larger than the nucleus, the physical size of the nucleus is lost, with the predominant surviving length scale being that of the neutron's reduced wave length. In this case, the $L\neq0$ absorption becomes irrelevant, while the L=0 absorption cross section becomes a fraction of $\pi\lambda\!\!\!^{-2}$. In the limit of the interaction potential being smoothly varying and always attractive, with a strong central absorptive region, the L=0 transmission coefficient would become unity with an absorption cross section of $\pi\lambda\!\!\!^{-2}$. However, the short-range nature of the nuclear potential invalidates the smoothly varying requirement, and for nuclear interactions a significant part of the incident wave is reflected, leaving the L=0 cross section significantly less than $\pi\lambda\!\!\!^{-2}$. Fig. VII.1 shows the relevant length scale for thermal-neutron interactions on isotopes with cross sections larger than ~1000 b. Notice than the largest absorption cross section is for thermal neutrons on ^{135}Xe. One of the main factors for this cross section being so high is the closure of the N=82 neutron shell to form an even-even nucleus. Even in this case, the absorption length scale is only ~1/3 of the maximum allowable value of the thermal-neutron's reduced wavelength. In the case of the virtual-photon lepton interaction we here assume the limiting cross section of $\pi\lambda\!\!\!^{-2}$.

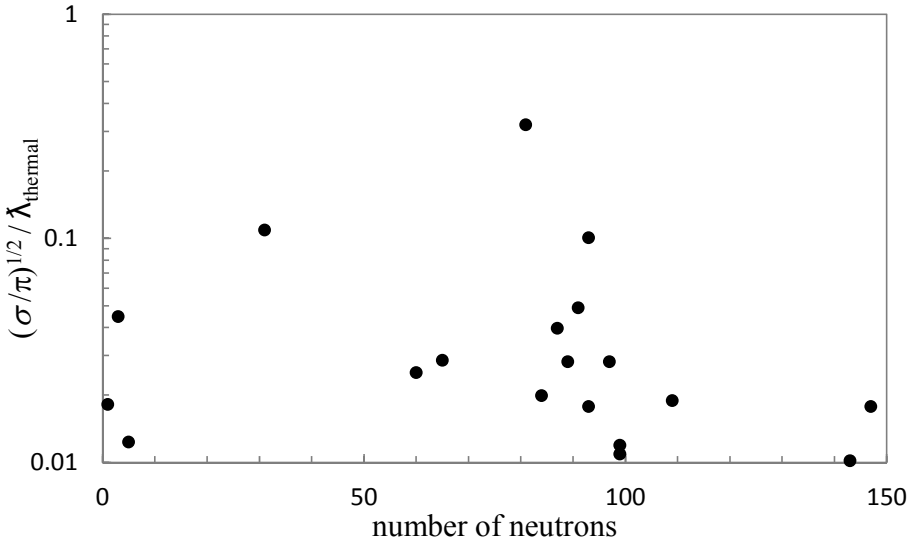

Fig. VII.1. Interaction length scale for thermal-neutron interactions with various nuclei, in units of the reduced wavelength of the corresponding neutrons (~0.3 Å).

VII.A Exchange of L=0 virtual photons

For the classical exchange of photons between a pair of micro black holes, both with fixed mass states, both the emission and absorption of the unphysical L=0 photons discussed above would be completely suppressed by energy conservation for isolated objects. We temporarily ignore this important fact and

use transition state theory to calculate the emission rate from a microscopic black hole where only L=0 emission is allowed [see Eq. (IV.C.17) for the emission from a macroscopic object], and obtain

$$R = \frac{1}{\pi\hbar}\int_0^\infty \exp(-\varepsilon/T_{\rm bh})\, d\varepsilon\,. \tag{VII.A.1}$$

The corresponding force between a pair of identical micro black holes would be

$$F = \frac{2}{\pi\hbar c}\int_0^\infty \varepsilon \exp(-\varepsilon/T_{\rm bh})\frac{\pi\lambda\!\!\!^{-2}}{4\pi d^2}\, d\varepsilon = \frac{\hbar c}{2\pi d^2}\int_0^\infty \exp(-\varepsilon/T_{\rm bh})\frac{d\varepsilon}{\varepsilon}\,. \tag{VII.A.2}$$

This force would be very large for small black holes with very high temperatures. The first step to obtaining a reasonable force strength is to realize, as discussed above, that the exchanges in Eq. (VII.A.2) violate conservation of energy and are not allowed if we assume classical physics. However, even though the emission and absorption ends of the exchanges violate energy conservation, exchanges can be allowed if they occur over times comparable to and/or shorter than those given by the time-energy uncertainty principle, $\tau = \hbar/(2\varepsilon)$. If we assume that the probability per unit time that the virtual exchanging photon is no longer available for an exchange is given by $1/\tau$, and that the relevant time scale is given by the photon transit time between the pair $t = d/c$, then the probability that an attempted exchange is successful is given by $\exp(-\varepsilon/T_{\rm ex})$ with an effective exchange temperature $T_{\rm ex} = \hbar c/(2d)$. Inspired by the previously discussed semi-classical photon emission models, we assume the $\exp(-\varepsilon/T_{\rm ex})$ needs to be replaced by the corresponding Planckian factor to obtain the correction result, and rewrite Eq. (VI.A.2) in the limit of large separations where $T_{\rm ex} << T_{\rm bh}$ as

$$F = \frac{\hbar c}{2\pi d^2}\int_0^\infty \frac{d\varepsilon}{\varepsilon[\exp(\varepsilon/T_{\rm ex})-1]}\,. \tag{VII.A.3}$$

In the limit of large separations, the repulsive force is independent of the black hole temperatures and thus independent of the masses of either micro black hole. If the force expressed by Eq. (VII.A.3) is assumed to be the origin of electromagnetism, then the fine structure constant can be expressed as

$$\alpha = \frac{1}{2\pi}\int_0^\infty \frac{1}{\varepsilon[\exp(\varepsilon/T_{\rm ex})-1]}\, d\varepsilon. \tag{VII.A.4}$$

These equations give an infinite force and an infinite fine structure constant. However, the origin of the divergence is the lowest-energy photons where $\lambda\!\!\!^{-} > d$, and thus the transmission coefficients used to obtain the relevant cross sections need to be modified to values lower than unity to correct for near-field effects.

VII.B Equivalence with exchanges stimulated by virtual-vacuum photons

In this section we will re-derive Eq. (VI.A.3) by instead considering the possibility that virtual-vacuum photons interact with charged leptons and/or micro black holes with a cross section of $\pi\lambda\!\!\!^{-2}$, and that the result of this interaction is the stimulated emission of an additional virtual photon. This process is depicted in Fig. VII.B.1. Given that the effective photon-particle interaction length is 2π times smaller than the photon's wave length, the stimulated emission is here assumed to not be correlated with the outgoing direction of the incident photon as in the case from objects that are much larger than the photon's wavelength (see section IV.D). The idea that black holes (or black-hole-like objects) can be stimulated to emit photons is not new. It has long been known that photons falling into a black hole cause a stimulated time-reversed emission with a probability of $\exp(-\varepsilon/T_{\rm bh})$ [BEK77]. In the limit of $T_{\rm ex} << T_{\rm bh}$ the probability becomes unity for all relevant photons, and thus if the incident photon comes

within ƛ of the black-hole-like object (in a semi-classical sense) then a stimulated-virtual photon is generated.

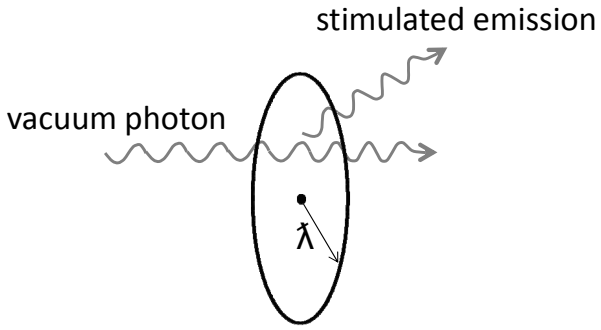

Fig. VII.B.1. Depiction of a virtual-stimulated emission generated by the passage of the virtual-vacuum photon within ƛ of a point particle. The wavelength of the schematic photons is not to scale.

The rate of stimulated virtual-photon production from an isolated particle can be obtained using Eq. (IV.D.5) by replacing the atomic cross section with $\pi ƛ^2$. The corresponding rate for generating stimulated-virtual photons is given by

$$R_S(\varepsilon) = \frac{\varepsilon^2 \sigma_a d\varepsilon}{\pi^2 \hbar^3 c^2} = \frac{\varepsilon^2 \pi ƛ^2 d\varepsilon}{\pi^2 \hbar^3 c^2} = \frac{\varepsilon^2 \hbar^2 c^2 d\varepsilon}{\varepsilon^2 \pi \hbar^3 c^2} = \frac{d\varepsilon}{\pi \hbar} \tag{VII.B.1}$$

This is a very simple and beautiful equation that is central to the results that follow.

The power of the stimulated emission from an isolated particle is obtained by integrating over Eq. (VII.B.1) multiplied by $\varepsilon = \hbar\omega$, and is given by

$$P_S = \int_0^\infty \frac{\varepsilon d\varepsilon}{\pi \hbar}. \tag{VII.B.2}$$

Of course, this stimulated emission violates conservation of energy, and is not allowed from an isolated fundamental particle. As discussed above, a violation of conservation of energy by an amount ε can be allowed for a time scale given by the time-energy uncertainty principle, $\tau = \hbar/(2\varepsilon)$. If, in this time scale, the stimulated emission could find a partner particle, then conservation of energy can be re-established and the exchange of the stimulated emission between a pair allowed. As previously discussed, we speculate that this exchange is the origin of the repulsive force between two identically charged leptons. Following some of the same logic used in section VII.A, Eq. (VII.B.2) can be used to obtain the repulsive force between two particles

$$F = \frac{2}{\pi \hbar c} \int_0^\infty \frac{\varepsilon}{[\exp(\varepsilon / T_{ex}) - 1]} \frac{\pi ƛ^2}{4\pi d^2} d\varepsilon = \frac{\hbar c}{2\pi d^2} \int_0^\infty \frac{d\varepsilon}{\varepsilon [\exp(\varepsilon / T_{ex}) - 1]} \ . \tag{VII.B.3}$$

This is the same result as Eq. (VII.A.3) and thus also leads to Eq. (VII.A.4).

VII.C High energy cutoff, particle size and mass, and *F=ma*

A comparison of Eq. (VII.B.1) with results from section VII.A and to transition state theory, implies particles have an infinite temperature. This unphysical result is a consequence of the incorrect assumption (used in section VII.B) that the stimulated-emission cross section of $\pi ƛ^2$ is valid for all incident virtual-photon energies, even those much larger than the rest-mass energy of the particle. As per our discussion on the Lamb shift, this cannot be the case (see section III.C) as the interaction cross section must fall to zero for virtual-photon energies much larger than the particle's mass, else the Lamb

shift would be infinite. But what is the nature of the transition to zero cross section? What is the transition energy? What functional form does it take? A traditional assumption used in previous semi-classical calculations [BJO64] has been to assume a sharp transition to zero at $\varepsilon \sim mc^2$. Here, we will argue for a different transition. Thinking semi-classically as in section III.C on the Lamb shift, virtual-vacuum photons can interact fully with (i.e. shake) a charged lepton when the wavelength is much larger than the particle's effective size ($\sim \lambda > ƛ_C$). However, when the wavelength becomes smaller than the particle's size, then different parts of the high frequency wave are trying to push different parts of the "particle" in opposite directions, and thus the overall strength of the total interaction decreases. Given that the characteristic particle length scale is the reduced Compton wavelength, which is the reduced wavelength of a photon containing the rest-mass energy of the particle of interest, we expect the transition to occur at a photon wavelength of $\lambda \sim \hbar c/(mc^2)$, and thus at a photon energy of $\sim 2\pi mc^2$. This logic is relatively vague, and should not be believed unless backed up by additional arguments.

Switching to a photon (particle) based model, the rate at which virtual-vacuum photons pass within ƛ of a particle is given by (VII.B.1), and thus the mean time between interactions, for a given plane of polarization, is given by

$$\tau = \frac{2\pi\hbar}{\int_0^{\varepsilon_c} d\varepsilon} = \frac{2\pi\hbar}{\varepsilon_c}, \tag{VII.C.1}$$

where ε_c is the cutoff energy below which we assume only one photon is trying to push the particle about in a given plane of polarization, at a given time. Above this energy cutoff, we assume that the presence of multiple photons cause the influence of the additional higher energy photons to have little effect. The cutoff energy can be estimated by setting Eq. (VII.C.1) to the transit time of a single photon across the particle's reduced Compton wavelength, giving $\varepsilon_c = 2\pi mc^2$ (the same result as obtained above).

Additional support for an effective cutoff at $\varepsilon_c = 2\pi mc^2$ can be obtained because this leads to an understanding of the presence of a finite rest mass of particles, and a better semi-classical explanation of the Lamb shift (see section III.C). If the process depicted in Fig. VII.B.1 is correct, in conjunction with the above discussed cutoff, then the power of the stimulated-virtual-photon production from an isolated particle is modified from Eq. (VII.B.2). As previously discussed, this emission is not allowed if only classical physics is applied. However, in quantum mechanics each photon emission is allowed for a time scale of $\hbar/(2\varepsilon)$. If we assume (as done previously) that the probability per unit time that the stimulated-virtual photon is no longer available for an exchange is $2\varepsilon/\hbar$, then the probability that it is lost to the exchange process at time t after its generation is $\exp(-2\varepsilon \cdot t/\hbar)$. The additional virtual-photon energy (above the virtual-photon vacuum ground-state energy) associated with the presence of an isolated particle can then be expressed as

$$\begin{aligned} E_s &= \int_0^{\varepsilon_c} \int_0^{\infty} \frac{\varepsilon}{\pi\hbar} \frac{t \exp(-2\varepsilon t/\hbar) dt}{\int_0^{\infty} \exp(-2\varepsilon t/\hbar) dt} d\varepsilon \\ &= \int_0^{\varepsilon_c} \int_0^{\infty} \frac{2\varepsilon^2}{\pi\hbar^2} t \exp(-2\varepsilon t/\hbar) dt\, d\varepsilon = \frac{1}{2\pi} \int_0^{\varepsilon_c} d\varepsilon = \frac{\varepsilon_c}{2\pi} = mc^2. \end{aligned} \tag{VII.C.4}$$

Sharp cutoffs are, of course, not physical. However, we here apply the philosophy that if a simplistic approach appears to work then we shall keep it until a more sophisticated one is needed.

The logic presented here does not explain the size of the particular particle's mass, but does give a physical mechanism for the existence of the rest mass, as the energy tied up in the cloud of stimulated-virtual photons surrounding an isolated particle. In this explanation, a given effective size defines an

effective high-energy photon cutoff, and this cutoff leads to a rest mass of $\varepsilon_c/(2\pi) = mc^2$, which is then consistent with the originally assumed effective size. Similarly, one could assume that the high-energy cutoff was the more fundamental quantity, and this leads to a mass equal to the reduced cutoff energy, which in turn leads to an effective size consistent with the assumed cutoff.

The high-energy photon cutoff of $\varepsilon_c = 2\pi mc^2$, and the low-energy cutoff used to obtain Eq. (III.C.15) solve several problems. As discussed above, the high-energy cutoff leads to a simple interpretation that the rest-mass energy is stored in the virtual-stimulated photons that surround massive particles. This interpretation has no problem with point particles, unlike the storage in the electric field surrounding a classical point particle. These cutoffs led to an effective particle size of ~ $\lambda\!\!\!^{-}_C/5.219$ as inferred by a massive particle's ability to sense the electron as obtained by the Lamb shift analysis in section III.C. If we assume this size smoothly matches in with the properties of non-micro black holes ($T_{bh}=8\pi m$ and $r_S=2m$) then it seems reasonable to suggest the size of particles around the Planck mass might be given by (in Planckian units)

$$r \sim \frac{1}{5.22 \cdot m} + 2m \,. \tag{VII.C.5}$$

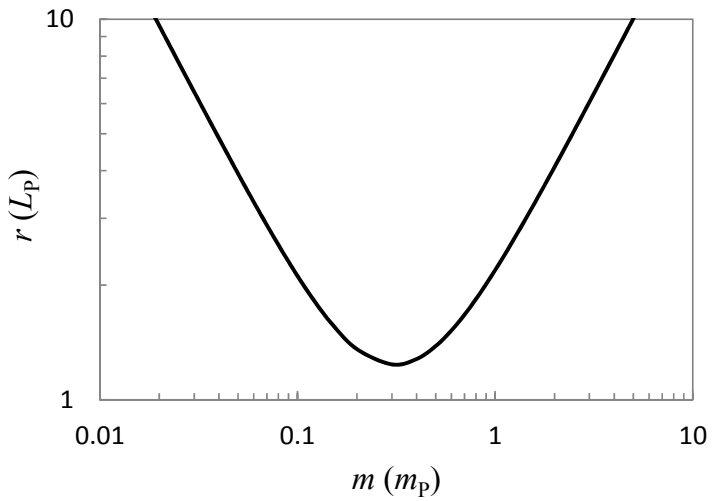

Fig. VII.C.1. Suggested relationship between particle size and mass. All units are Planckian ($\hbar = c = G = 1$).

Particle size is displayed as a function of particle mass around the Planck mass in Fig. VII.C.1. Notice that a particle's effective size never falls below the Planck length. Assuming the effective particle size of ~$\lambda\!\!\!^{-}_C/5.219$ smoothly matches into the size of black holes with masses above the Planck mass is assuming an intimate connection between leptons and black holes, and in particular assumes small black holes are made fuzzy by the emission and absorption of virtual photons.

The above-discussed concept of the particle's mass being contained in a surrounding cloud of virtual photons naturally gives the relativistic mass of a particle as a function of relative velocity because of the different rates of the passage of time between different inertial frames that control the time-energy uncertainty principle. Similarly, in a gravitational field, where the rate of the passage of time changes with height, the uncertainty principle modifies the emission and reabsorption process as a function of the angle to the gravitational field. This causes a force of $F = mg$ in the direction where the passage of time is the slowest. Although these concepts automatically give $F = ma$ in the low-energy limit, it might be of interest to some to see how the concept of virtual-photon emission and reabsorption, by the same particle, gives a clear semi-classical picture of why a force is required to maintain a fixed acceleration

and why the proportionality constant is the mass. This result can be obtained by first assuming that the emitted virtual photons of energy ε can travel half their reduced wavelength in a time $\hbar/(2\varepsilon)$. If the self-absorption (return) of these virtual photons is assumed to take the same amount of time then the emission and self-absorption process can be considered to take a total time of $\hbar/\varepsilon$. If the particle is experiencing a uniform acceleration of a, then the velocity change between the emission and self-absorption times is given by $a\hbar/\varepsilon$. The corresponding Doppler shift causes a change in the momentum between the emitted and self-absorbed photons as viewed by the accelerating particle. For photons emitted in the direction of the acceleration (or in the opposite direction) the momentum change for a single emission and self-absorption is $a\hbar/c^2$ (in the non-relativistic limit) and independent of the photons energy. Averaging over all possible emission orientations causes a drop in the average momentum change by a factor of two to $a\hbar/(2c^2)$ per emission. To obtain the average rate of momentum change ($\mathrm{d}P/\mathrm{d}t$) we need only multiply by the rate of virtual-photon emission $R = \varepsilon_c/(\pi\hbar)$. This gives $\mathrm{d}P/\mathrm{d}t = a\hbar/(2c^2)\cdot\varepsilon_c/(\pi\hbar) = a\varepsilon_c/(2\pi c^2)$. Therefore, to maintain a constant acceleration, a force must be applied equal to $F=ma$ (here we have assumed the high-energy photon cutoff is at $\varepsilon_c = 2\pi mc^2$).

VII.D Near-field effects and the removal of the infinity (low-energy cutoff)

To remove the infinity from Eq. (VII.A.3) we need to consider how the photon-particle interaction cross section is altered when the incoming photon does not start from a source particle an infinite distance from the absorbing particle. Some estimates of these near-field corrections can be obtained via simple semi-classical arguments. For example, based on the assumed interaction cross section of $\pi\lambda\!\!\!^{-2}$, each lepton and/or micro black hole can be thought of as a sphere of radius $\lambda\!\!\!^{-}$ when interacting with a photon with a reduced wavelength of $\lambda\!\!\!^{-}$. Within this simple picture, near-field effects should start growing as the separation decreases through ~$2\lambda\!\!\!^{-}$ (as the two semi-classical spheres start to overlap), and be strong for photons exchanged between particles separated by $d < \lambda\!\!\!^{-}$, with the virtual photons increasingly losing their ability to interact with the particles (as individual objects) as the separation distance decreases towards zero. This behavior is analogous to the interaction properties of closely spaced classical antennas [IRA08].

We write the near-field corrected interaction cross section as $\sigma_{nf} = f_{nf}(\lambda\!\!\!^{-},d)\cdot\pi\lambda\!\!\!^{-2}$, where $f_{nf}(\lambda\!\!\!^{-},d)$ is the near-field absorption correction factor. Given the above simple arguments, it seems reasonable that a rough estimate of the universal charge could be obtained by setting $f_{nf}(\lambda\!\!\!^{-},d) = 0$ for $\lambda\!\!\!^{-} > d$, and otherwise unity for $\lambda\!\!\!^{-} \le d$. Using Eq. (VII.A.4) and switching to energy in units of the exchange temperature, $T_{ex} = \hbar c/(2d)$, where the point $\lambda\!\!\!^{-}=d$ corresponds to $\varepsilon=2$, we can write

$$\alpha \sim \frac{1}{2\pi}\int_2^\infty \frac{1}{\varepsilon[\exp(\varepsilon)-1]}\,d\varepsilon \sim 1/119. \qquad \text{(VII.D.1)}$$

The corresponding estimate of the fundamental unit of charge is ~1.72×10^{-19} C.

A quantitative estimate of near-field-like effects was obtained by Bethe [BET44], who considered the transmission of electromagnetic radiation through a hole of radius a in a conducting sheet. At first, this problem may seem far removed from the question at hand, until one realizes that when the radius of the hole is small compared to $\lambda\!\!\!^{-}$, then the incident photons are effectively absorbed and then re-emitted by the conducting material surrounding the hole. This is analogous to the near-field correction that must be added to Eq. (VII.A.4) where virtual photons are first emitted from one particle and absorbed by a nearby partner. The value of $\lambda\!\!\!^{-}/a$ in the transmission problem considered by Bethe is analogous to, but not exactly the same as, the value $\lambda\!\!\!^{-}/d$ in the near-field problem considered here. Bethe found that when

$\lambda\!\!\!^{-} >> a$, the effective cross-sectional area of the hole corresponding to the transmission (absorption and emission) of electromagnetic radiation is given by

$$\sigma = \frac{64}{27\pi^2}\left(\frac{a}{\lambda\!\!\!^{-}}\right)^4 \pi a^2. \qquad \text{(VII.D.2)}$$

If we assume that the combined emission and absorption near-field correction factor needed in the present work is approximately the same as that obtained by Bethe, but with the radius of the hole in the conducted sheet replaced by the distance between the emitting and absorbing particle pair, then the total near-field scaling to be added to Eq. (VII.A.4) will be $\sim 4\varepsilon^4/(27\pi^2)$ for $\varepsilon < \varepsilon^* = (27\pi^2/4)^{1/4}$ (see Fig. VII.D.1) and thus (remember ε is here in units of T_{ex})

$$\alpha \sim \frac{1}{2\pi}\left[\int_0^{\varepsilon^*} \frac{4\varepsilon^3}{27\pi^2[\exp(\varepsilon)-1]}\,d\varepsilon + \int_{\varepsilon^*}^{\infty} \frac{1}{\varepsilon[\exp(\varepsilon)-1]}\,d\varepsilon.\right] = 1/122. \qquad \text{(VII.D.3)}$$

The corresponding estimate of the fundamental unit of charge is $\sim 1.70\times10^{-19}$ C. Here, we have made the simplifying assumption that the near-field correction can only be less than or equal to unity.

We assume the estimates of the fundamental unit of charge given by Eq.s (VII.D.1) and (VII.D.3) are a little high because the corresponding assumed total near-field scaling applied to Eq. (VII.A.3) does not smoothly approach unity at $\varepsilon > 4$ (near $d \sim 2\lambda\!\!\!^{-}$) as suggested by the simple arguments given above. To correct for this weakness we assume the virtual-photon interaction cross section of $\pi\lambda\!\!\!^{-2}$ for an isolated particle implies that a semi-classical distribution of photon-interaction sites exist around each particle. Guided by the Gaussian distribution of the matter (particle) core of a lepton generated by its interaction with the vacuum photons (see section III.C on the Lamb shift), we assume the distribution of photon-interaction sites is also Gaussian (the ground-state wave function of a harmonic oscillator). To obtain the required photon-particle interaction size of $\lambda\!\!\!^{-}$, we set the distribution of interaction sites to

$$\psi(r,\lambda\!\!\!^{-}) \propto \exp\left(\frac{-r^2}{2\lambda\!\!\!^{-2}}\right). \qquad \text{(VII.D.4)}$$

For a semi-classical virtual photon making an attempted transition between a pair of particles separated by a distance d, we assume the amplitude per unit length for absorption is given by the density of the absorption sites along the classical path joining the particle pair, as given by Eq. (VII.D.4). This assumption leads to a near-field absorption correction factor of

$$f_{nf}(\lambda\!\!\!^{-},d) = \left|\frac{2}{\lambda\!\!\!^{-}\sqrt{2\pi}}\int_0^d \exp\left(\frac{-r^2}{2\lambda\!\!\!^{-2}}\right)dr\right|^2 = \mathrm{erf}^2\left(\frac{d}{\lambda\!\!\!^{-}\sqrt{2}}\right). \qquad \text{(VII.D.5)}$$

The corresponding modification to the absorption cross section is displayed by the solid curve in Fig. VII.D.2. Eq. (VII.D.5) provides a near-field correction that approaches zero and unity, in a smooth manner, as ε approaches zero and as ε moves above 4 times the exchange temperature (i.e. as $\lambda\!\!\!^{-}$ drops below $\sim 2d$).

To modify the calculation of the fine structure constant given by Eq. (VII.A.4) to include the near-field affects outlined by Eq. (VII.D.5), the cross section for the absorption of the stimulated-virtual photons must be multiplied by f_{nf}. Perhaps less obvious, is that the cross section used to calculate the emission rate of initiating the exchange must also be multiplied by f_{nf}. This is due to time-symmetry arguments that apply equally to emission and absorption processes [also see Eq. (VI.A.2)]. Including the near-field effects at both the initiation and completion ends of the photon exchanges gives the result

$$\alpha = \frac{1}{2\pi}\int_0^{\infty} \frac{\mathrm{erf}^4(\varepsilon/2^{3/2})}{\varepsilon[\exp(\varepsilon)-1]}\,d\varepsilon = 1/138.9099. \qquad \text{(VII.D.6)}$$

As done previously, Eq. (VII.D.6) is written with energy in units of T_{ex}. The corresponding calculated fundamental unit of charge is 1.591333×10^{-19} C. Fig. VII.D.1 compares the near-field correction obtained via the square of Eq. (VII.D.5) to that obtained by Bethe for the transmission of photons through a circular hole in a conducting sheet. Notice that the low energy dependence of the square of Eq. (VII.D.5) has the same ε^4 behavior as that obtained by Bethe, but a more realistic approach to unity near $4\varepsilon/T_{ex}$ (i.e. near $d\sim2\lambda\!\!\!^{-}$).

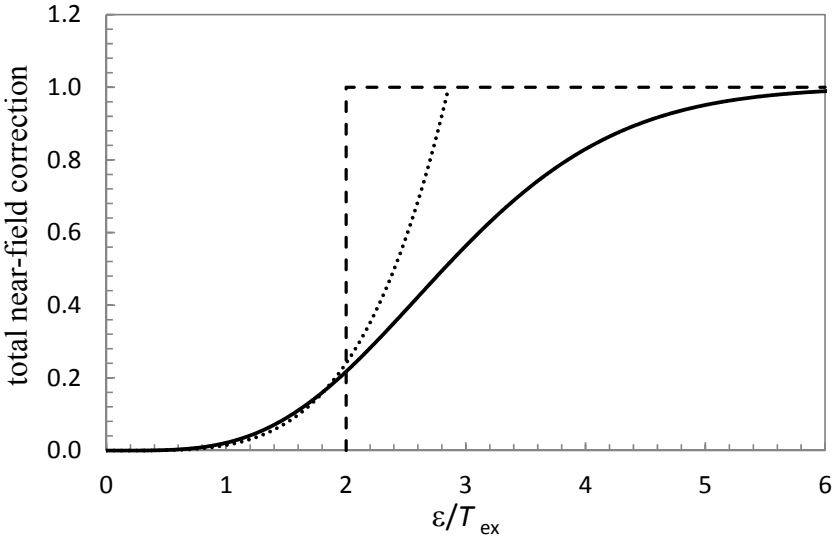

Fig. VII.D.1. Several estimates of the total near-field scaling factor that needs to be applied to Eq. (VII.A.4). The dashed line shows the simple approximation used to obtain Eq. (VII.D.1) where the total near-field scaling factor is assumed to be zero for $\varepsilon<2$ (in units of T_{ex}) and otherwise unity. The dotted curve displays the estimate based on the absorption and emission of photons through a hole in a conducting sheet [BET44] used to obtain Eq. (VII.D.3). The solid curve shows the estimate based on Eq. (VII.D.5) which leads to a fundamental unit of charge of 1.6×10^{-19} C [see Eq. (VII.D.6)].

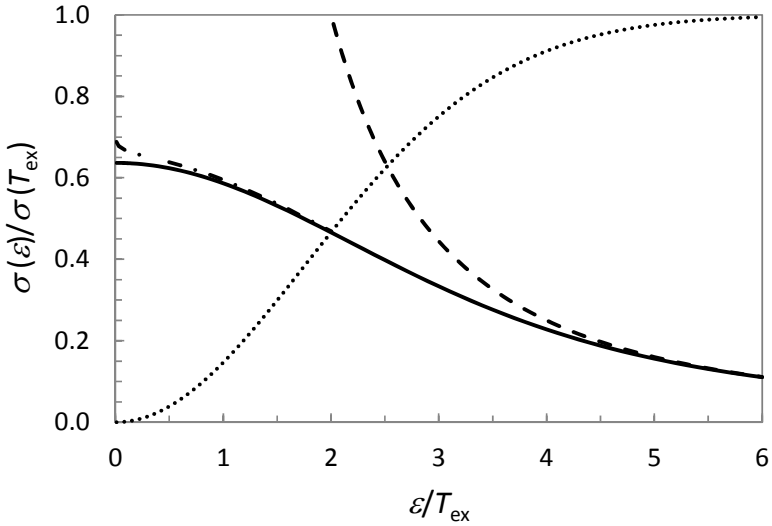

Fig. VII.D.2. Effective interaction cross sections (solid curve) obtained using the near-field absorption correction factor represented by Eq. (VII.D.5) (dotted curve). At $\varepsilon/T_{ex}=2$ and 4, the separations between emitter and absorber are $\lambda\!\!\!^{-}$ and $2\lambda\!\!\!^{-}$, respectively. The dashed curve displays the far-field result. The dashed-dotted curve displays the higher-order correction discussed in section VII.E.

The force associated with the semi-classical exchange of virtual photons between two particles represented by Eq. (VII.D.6) can only generate repulsion. However, an attractive force between oppositely charged particles can be obtained by assuming the opposite charge is associated with a hole in a Fermi-sea of negative-energy particles [BJO64, chap. 5].

VII.E Speculative higher order QED-like corrections

The near-field correction factor as expressed by Eq. (VII.D.5) does not adequately reproduce the fine structure constant obtained via experiment [MOH15]. Therefore, if Eq. (VII.D.6) is on the right track, it needs to be modified. We suggest that a possible source for a modification is higher-order QED corrections to the near-field correction factor, especially for $d < \lambda\!\!\!^{-}$. For particle separation distances $d >> \lambda\!\!\!^{-}$, where the low-order correction from Eq. (VII.D.5) is small, we expect the higher-order QED corrections to be very small. However, with decreasing d, we expect higher-order effects associated with the QED structure of the particles to grow logarithmically. We suggest the functional form for the higher-order near-field absorption correction factor is

$$f_{\rm nf}(\alpha) = f_{\rm nf}(1 - \alpha \ln(f_{\rm nf})), \tag{VII.E.1}$$

where $f_{\rm nf}$ is the non-QED scaling of the absorption cross section as given by Eq. (VII.D.5). The corresponding modification to the absorption cross section is displayed by the dashed-dotted curve in Fig. VII.D.2. Substituting Eq. (VII.D.5) into Eq. (VII.E.1) and then into Eq. (VII.D.6) gives

$$\alpha = \frac{1}{2\pi}\int_0^\infty \frac{\mathrm{erf}^4(\varepsilon/2^{3/2})[1 - \alpha \ln(\mathrm{erf}^2(\varepsilon/2^{3/2}))]^2}{\varepsilon[\exp(\varepsilon) - 1]}\, d\varepsilon\,. \tag{VII.E.2}$$

This equation can be solved numerically by iteration. The calculated inverse fine structure constant and corresponding fundamental unit of charge are 137.0355 and 1.602180×10^{-19} C, respectively. The calculated fundamental unit of charge differs from the corresponding value inferred from experiment [MOH15] by 1 part in 5 million.

If Eq. (VII.E.1) and (VII.E.2) are on the right track, it is likely that even higher-order corrections exist, with the α inside the integral of Eq. (VII.E.2) needing to be replaced by $\alpha + a\alpha^2 + b\alpha^3 + \ldots$. Based on the higher-order corrections to other QED calculated qualities, it is not unreasonable to suggest a might lie in the range from $-1/\pi$ to $1/\pi$. This range gives an inverse fine structure constant of 137.036 ± 0.004 and a corresponding fundamental unit of charge of $(1.60218\pm0.00005)\times10^{-19}$ C. The agreement with experiment does not prove that Eq. (VII.E.2) is correct, but demonstrates, that with reasonable suggestions for near-field corrections and high-order corrections thereof, the mechanism for generating the fundamental unit of charge described here can be made to work. Obviously additional work is needed to obtain more quantitative estimates of the near-field corrections.

VIII. Summary and conclusions

A review of several semi-classical methods for estimating the properties of photon emission from hot objects (including black holes) demonstrates that the corresponding expressions often contain a simple exponential term $\exp(-\varepsilon/T)$. In order to obtain the correct emission rates for photons, this exponential term often needs to be replaced with the corresponding Planckian factor $[\exp(\varepsilon/T)-1]^{-1}$. This replacement is associated with the existence of stimulated emission. The concept of stimulated emission is here extended to fundamental particles. This leads to several promising results simple enough to be explained to an undergraduate physics audience.

By assuming virtual-vacuum photons can stimulate an isolated charged lepton to emit additional virtual photons with a cross section of $\pi\lambda\!\!\!^{-2}$, and invoking a high-energy cutoff of $2\pi mc^2$, beyond which virtual photons no longer interact with a particle of mass m, then the additional energy associated with the cloud of stimulated virtual photons surrounding the particle is equal to the particle's rest-mass energy, mc^2. This storage of the rest-mass energy in the surrounding cloud of virtual photons is similar to the storage of the rest-mass in the surrounding classical electric field. The high-energy cutoff of $2\pi mc^2$, in conjunction with a modification of the traditional low-energy cutoff used in semi-classical calculations of the Lamb shift, leads to a calculated hydrogen Lamb shift of 1057.87 MHz, in agreement with experiment to ~ 1 part in 10^5. The relativistic mass correction, and a simple understanding of why $F = ma$ in the non-relativistic limit, is also obtained.

An expression for the fine structure constant can be obtained if electromagnetism is assumed to be associated with the exchange of stimulated-virtual photons between particle pairs. Our first semi-classical estimate of the repulsive force generated by the exchange of virtual photons between a pair of particles, obtained using only the far-field interaction cross section of $\pi\lambda\!\!\!^{-2}$, is infinite. Including an estimate of near-field effects (to low order) obtained via simple arguments, leads to a force that defines a fundamental unit of charge of $\sim 1.6\times10^{-19}$ C. An educated guess for higher-order corrections to near-field effects gives an inverse fine structure constant of $1/\alpha = 137.04$ and a corresponding calculated charge of 1.6022×10^{-19} C. The semi-classical choices needed to obtain this result are: a far-field cross section of $\pi\lambda\!\!\!^{-2}$ for the generation of stimulated virtual-photon emission; a probability per unit time that stimulated virtual photons are no longer available for an exchange with a neighboring particle, set by the time-energy uncertainty principle; the substitution of an exponential with the corresponding Planckian factor; and near-field effects controlled by a Gaussian distribution of photon interaction sites surrounding charged particles with higher-order corrections as given by Eq. (VII.E.1). Obviously, more work on photon-particle near-field corrections is needed. If the semi-classical choices made here can be justified by detailed calculations, then an understanding of the numerical value of the fine structure constant may emerge. The present study suggests charge is an emergent property generated by a simple interaction mechanism between point-like particles and the electromagnetic vacuum, similar to the process that generates the Lamb shift.

Appendix A. Photon clustering from black bodies by semi-classical means

Spontaneously emitted photons are not "magically" generated at the surface of black bodies, but must be emitted from a site of excitation within the black body a path length x_0 from the surface in the direction of the emission. Given this emission site is within the black body, there is a probability that the spontaneously emitted photon is absorbed during its attempt to escape through the surface. For convenience, we operate in length units equal to the mean-free path for photon absorption. Ignoring the possibility of stimulated emission, the spontaneously emitted photon is either emitted with a probability $\exp(-x_0)$ or absorbed with a probability of $1-\exp(-x_0)$. Including stimulated emission, there is a probability that a spontaneously emitted photon will pass near a site of excitation and cause the stimulated emission of an additional photon. There are thus two types of interaction sites for the exiting photons to encounter: sites which can absorb the photon by making a transition from state s_a to state s_b; and those that can be stimulated to emit a photon by the transition of state s_b to state s_a. These states are separated by an energy difference of ε. As discussed in section IV, the absorption cross section is equal to the corresponding stimulated emission cross section. However, the ratio of the number of sites in state s_b available for stimulated emission to the number of sites in state s_a available for absorption, is given by

$f = \exp(-\varepsilon/T)$, where T is the temperature of the body. The mean-free path for stimulated emission is thus $1/f$, and the total mean-free path including both absorption and stimulated emission is $1/(1+f)$. We do not consider a scattering cross section because, for a surface to be a perfect black body, there must be no scattering term.

To calculate the probabilities of all the different manners in which a spontaneously emitted photon can escape and/or generate stimulated photons [LES08b] we consider the probability that i interactions occur at distances $x_1, x_2, \ldots, x_i$ from the surface, and that the number of photons after each interaction is $n_1, n_2, \ldots, n_i$. For example, a spontaneously emitted photon generated at x_0 might be absorbed at x_1 with $n_1=0$; or the interaction at x_1 could be stimulated to emit with $n_1=2$ with no further interactions and with two photons exiting the surface as a correlated pair. Two possible event sequences are depicted in Fig. A.1.

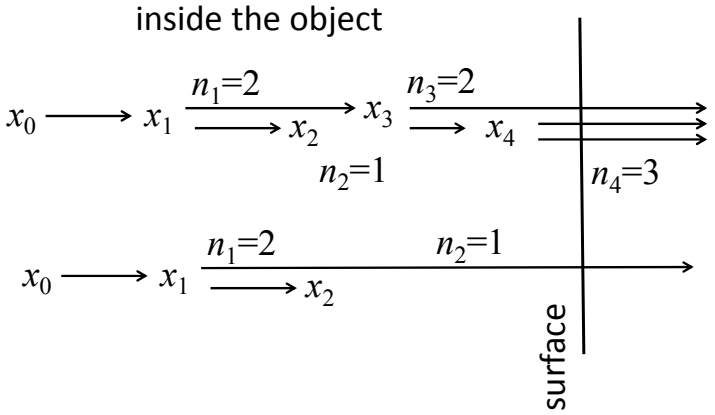

Fig. A.1. Some possible event sequences for the emission of photons from a surface.

Immediately, several rules are self-evident for events containing i interaction sites:

$$\begin{aligned} &n_1, n_2, \ldots, n_{i-1} > 0, \\ &n_i \text{ can be an integer from } 0 \text{ to } i+1, \\ &\left|\Delta n_j\right| = \left|n_j - n_{j-1}\right| = 1, \\ &\Delta n_j = n_j - n_{j-1} = \pm 1 \quad (+1 \text{ for stimulated emission, and } -1 \text{ for absorption}). \end{aligned} \tag{A.1}$$

Given the relative mean free paths quoted above, if an interaction occurs, the probability for the Δn_j are

$$P(\Delta n_j = -1) = \frac{1}{1+f} = q \text{ and } P(\Delta n_j = +1) = \frac{f}{1+f} = p, \tag{A.2}$$

with $q + p = 1$, and $p/q = f$.

Consider n photons traversing a very thin element of the surface of thickness $1/m$. The probabilities of n, n+1, and n−1 photons exiting the element are

$$P(\Delta n = -1) = \frac{n}{m}; \quad P(\Delta n = +1)\frac{n}{m} f; \quad \text{and} \quad P(\Delta n = 0) = 1 - \frac{n}{m}(1+f). \tag{A.3}$$

The probability that nothing happens in traversing a thick element from x_i to x_j is therefore given by

$$P(\text{nothing happens from } x_i \to x_j) = \lim_{m\to\infty}\left(1 - \frac{n}{m}(1+f)\right)^{(x_i - x_j)m} = \exp[-(x_i - x_j)n(1+f)]. \tag{A.4}$$

Remember the x_i are the interaction depths, and thus for a photon heading toward the surface $x_j < x_i$. The probability of i interaction sites with a specific pattern of photon numbers $n_1,\ldots,n_i$ after each interaction

with a starting spontaneous emission a path length x_0 from the surface, and interaction sites at $x_1,\ldots,x_i$ with $x_0 > x_1 > x_2 \ldots > x_i$, is then given by

$$P(i,x_0,...x_i,n_1,...n_i) = e^{-(x_0-x_1)(1+f)} S_1 e^{-(x_1-x_2)n_1(1+f)} n_1 S_2 e^{-(x_2-x_3)n_2(1+f)} \ldots e^{-(x_{i-1}-x_i)n_{i-1}(1+f)} n_{i-1} S_i e^{-(x_i)n_i(1+f)}, \quad \text{(A.5)}$$

where $S_j = f \cdot dx_j$ for $\Delta n = n_j - n_{j-1} = 1$ (stimulated emission at x_j), and $S_j = dx_j$ for $\Delta n = -1$ (absorption at x_j). The emission rate (normalized to the rate for emission from the surface of the original spontaneous emission excluding the effects of stimulated emission, i.e. the classical emission rate) for generating events with n_i photons at the surface after i interactions with a specific pattern of $n_1,\ldots,n_i$ is then

$$\begin{aligned} R(i,n_1,...n_i) &= \left(\prod_{j=1}^{i}\frac{S_j}{dx_j}\right)\left(\prod_{k=1}^{i-1} n_k\right)\int_{x_0=0}^{\infty}\int_{x_1=0}^{x_0}\ldots\int_{x_i=0}^{x_{i-1}} e^{-(x_0-x_1)(1+f)}\left(\prod_{l=1}^{i-1} e^{-(x_l-x_{l+1})n_l(1+f)}\right)e^{-x_i n_i(1+f)}dx_i\ldots dx_0 \\ &= \left(\prod_{j=1}^{i}\frac{S_j}{dx_j}\right)\left(\prod_{k=1}^{i-1} n_k\right)\frac{1}{(1+f)^{i+1}}\frac{1}{\prod_{l=1}^{i} n_l} = \frac{f^a}{(1+f)^{i+1}}\frac{1}{n_i} = \frac{q^{i+1}}{n_i}\left(\frac{p}{q}\right)^a \end{aligned} \quad \text{(A.6)}$$

where $a \le i$ is the number of interaction sites involving stimulated emission. The number of exiting photons is $n_i = 1 + a - (i-a) = 1 + 2a - i$, and thus $a = (n_i + i - 1)/2 \le i$ and $i \ge n_i - 1$. We can then rewrite Eq. (A.6) as

$$R(i,n_1,...n_i) = \frac{q}{n_i} p^a q^{i-a} = \frac{q}{n_i} p^{(n_i+i-1)/2} q^{i-(n_i+i-1)/2} = \frac{q}{n_i} p^{(n_i+i-1)/2} q^{(i-n_i+1)/2}. \quad \text{(A.7)}$$

The relative rate of emission for events containing n correlated photons to the rate of emission of classical single photons is then

$$R(n) = \frac{q}{n}\sum_{i=n-1}^{\infty}[i \to n] p^{(n+i-1)/2} q^{(i-n+1)/2}, \quad \text{(A.8)}$$

where $[i \to n]$ is the number of ways of arranging the n_1, $n_2 \ldots n_{i-1}, n_i = n$ with the number of photons after the i^{th} interaction equal to n.

Table A.1. The probability of getting to j after $i < 10$ steps in an asymmetric random walk starting at $j = 1$, with the probability of a unit step to higher (lower) j equal to p (q), with a walk-terminating boundary at $j = 0$.

j	Probability $W(i,j)$									
10										p^9
9									p^8	
8								p^7		$8p^8q$
7							p^6		$7p^7q$	
6						p^5		$6p^6q$		$27p^7q^2$
5					p^4		$5p^5q$		$20p^6q^2$	
4				p^3		$4p^4q$		$14p^5q^2$		$48p^6q^3$
3			p^2		$3p^3q$		$9p^4q^2$		$28p^5q^3$	
2		p		$2p^2q$		$5p^3q^2$		$14p^4q^3$		$42p^5q^4$
1	1		pq		$2p^2q^2$		$5p^3q^3$		$14p^4q^4$	
0		q		pq^2		$2p^2q^3$		$5p^3q^4$		$14p^4q^5$
i	0	1	2	3	4	5	6	7	8	9

From Eq. (A.8) we see that the passage of photons through a black body is related to an asymmetric random walk starting at the number of photons $j = 1$ with probabilities of a unit step to higher and lower j

equal to p and q, respectively, and with an absorptive boundary at $j=0$. If the random walk gets to $j=0$, it is terminated. The probabilities of getting to j after $i<10$ steps are listed in Table A.1. The combinational factors in front of the $p^{(j+i-1)/2}q^{(i-j+1)/2}$ terms listed in Table A.1 are the same combinational factors needed to evaluate Eq. (A.8), and we write the random walk probabilities as

$$W(i,j)=[i\to j]p^{(j+i-1)/2}q^{(i-j+1)/2}. \tag{A.9}$$

For a system in thermodynamic equilibrium, the probability that a given photon will induce a stimulated emission is less than the probability that it will be absorbed, and thus $p < q$. Applying this constant to the asymmetric random walk leads to the results that in the limit as the number of steps $i\to\infty$, all paths end at $j=0$. We can therefore write

$$\sum_{i=1}^{\infty}W(i,0)=\sum_{i=1}^{\infty}[i\to 0]p^{(i-1)/2}q^{(i+1)/2}=1. \tag{A.10}$$

Properties of the combinatorial factors $[i\to j]$ include

$$\begin{aligned}
&[0\to 1]=[1\to 0]=1.\\
&[i\to j]=0 \quad \text{if } i<j-1, \text{ or if } i \text{ and } j \text{ are both even, or if } i \text{ and } j \text{ are both odd.}\\
&[j-1\to j]=1.\\
&[i+1\to j]=[i\to j-1]+[i\to j+1] \qquad \text{if } j\ge 2.\\
&[i\to 2]=[i+1\to 1]=[i+2\to 0].\\
&[i\to 1]=[i+1\to 0].
\end{aligned} \tag{A.11}$$

From Eq.s (A.8), (A.10) and (A.11) we can write the relative emission rate for a single uncorrelated photon from a black body (including the effects of stimulated emission) as

$$R(1)=q\sum_{i=0}^{\infty}[i\to 1]p^{i/2}q^{i/2}=\sum_{i=0}^{\infty}[i+1\to 0]p^{i/2}q^{(2+i)/2}=\sum_{i=1}^{\infty}[i\to 0]p^{(i-1)/2}q^{(i+1)/2}=1. \tag{A.12}$$

i.e. the emission rate of uncorrelated photons is unchanged by the inclusion of stimulated emission. Similarly we can write the relative emission rate for correlated photon pairs as

$$\begin{aligned}
R(2)&=\frac{q}{2}\sum_{i=1}^{\infty}[i\to 2]p^{(i+1)/2}q^{(i-1)/2}=\frac{1}{2q}\sum_{i=1}^{\infty}[i+2\to 0]p^{(i+1)/2}q^{(i+3)/2}=\frac{1}{2q}\sum_{i=3}^{\infty}[i\to 0]p^{(i-1)/2}q^{(i+1)/2}\\
&=\frac{1}{2q}\left\{\left(\sum_{i=1}^{\infty}[i\to 0]p^{(i-1)/2}q^{(i+1)/2}\right)-q\right\}=\frac{1-q}{2q}=\frac{f}{2}.
\end{aligned} \tag{A.13}$$

To obtain $R(n)$ for all $n > 2$ we define the photon-emission rate associated with all events with n correlated photons

$$M(n)=nR(n)=q\sum_{i=n-1}^{\infty}[i\to n]p^{(n+i-1)/2}q^{(i-n+1)/2}=qp^{n-1}+q\sum_{i=n+1}^{\infty}[i\to n]p^{(n+i-1)/2}q^{(i-n+1)/2}, \tag{A.14}$$

and can thus write

$$\begin{aligned}
M(n+1)&=q\sum_{i=n}^{\infty}[i\to n+1]p^{(i+n)/2}q^{(i-n)/2} \qquad \text{and}\\
M(n-1)&=q\sum_{i=n-2}^{\infty}[i\to n-1]p^{(i+n-2)/2}q^{(i-n+2)/2}.
\end{aligned} \tag{A.15}$$

We are here assuming $n>2$ and can therefore use the relationship $[i\to n]=[i-1\to n-1]+[i-1\to n+1]$, and modify Eq. (A.14) to

$$M(n) = qp^{n-1} + q^2 \sum_{i=n+1}^{\infty} [i-1 \to n-1] p^{(i+n-1)/2} q^{(i-n-1)/2} + q^2 \sum_{i=n+1}^{\infty} [i-1 \to n+1] p^{(i+n-1)/2} q^{(i-n-1)/2}$$

$$= qp^{n-1} + q\left\{ p \sum_{i=n+1}^{\infty} [i-1 \to n-1] p^{(i+n-3)/2} q^{(i-n+1)/2} + q \sum_{i=n}^{\infty} [i \to n+1] p^{(i+n)/2} q^{(i-n)/2} \right\}$$

$$= qp^{n-1} + q\left\{ p \sum_{i=n}^{\infty} [i \to n-1] p^{(i+n-2)/2} q^{(i-n+2)/2} + M(n+1) \right\} \tag{A.16}$$

$$= qp^{n-1} + qM(n+1) + qp\left\{ \left(\sum_{i=n-2}^{\infty} [i \to n-1] p^{(i+n-2)/2} q^{(i-n+2)/2} \right) - p^{n-2} \right\}$$

$$= qp^{n-1} + qM(n+1) + pM(n-1) - qp^{n-1} = qM(n+1) + pM(n-1).$$

We can thus rewrite

$$M(n+1) = \frac{M(n) - pM(n-1)}{q} = (1+f)\left\{ M(n) - \frac{f}{1+f} M(n-1) \right\} = (1+f)M(n) - fM(n-1). \tag{A.17}$$

We have already demonstrated that $M(1)=1$ and $M(2)=2R(2)=f$, and we now have via Eq. (A.17) $M(3) =(1+f)f-f=f^2$. Given these results, we set $M(n)=f^{n-1}$ for $n\leq 3$ and then using Eq. (A.17) we can write

$$M(n+1) = (1+f) f^{n-1} - f \cdot f^{n-2} = f^n. \tag{A.18}$$

and thus by induction we have proven $M(n)=f^{n-1}$ and $R(n)=f^{n-1}/n$ for all counting integers n. The rate of correlated photon emission relative to the uncorrelated photon-emission rate is then given by

$$\frac{\text{correlated}}{\text{uncorrelated}} = f + f^2 + f^3 + \ldots = \frac{f}{1-f} = \frac{\exp(-\varepsilon/T)}{1-\exp(-\varepsilon/T)} = \frac{1}{\exp(\varepsilon/T)-1}, \tag{A.19}$$

and thus the total emission rate to the uncorrelated rate is

$$\frac{\text{total}}{\text{uncorrelated}} = 1 + \frac{1}{\exp(\varepsilon/T)-1} = \frac{\exp(\varepsilon/T)}{\exp(\varepsilon/T)-1}. \tag{A.20}$$

This is the factor required to turn Eq. (IV.C.18) into the correct black body emission rate.

This was a long and complex method to get a result that is easily obtainable from quantum theory. However, it demonstrates that the semi-classical addition of stimulated emission into a semi-classical calculation of photon emission leads to photon-photon correlations and the correct quantum result for the total emission rate. In the next appendix we demonstrate that the semi-classical photon-photon correlations obtained in this appendix lead to the Hanbury Brown and Twiss effect for black bodies.

Appendix B. Hanbury Brown and Twiss effect for a black body by semi-classical means

The semi-classical photon-photon correlations from black bodies, inferred in Appendix A, lead to both photon-photon temporal and spatial correlations in agreement with the Hanbury Brown and Twiss effect. The corresponding derivation is presented below. This result is of importance to the discussions in section VII, because it has been determined that black holes can also be stimulated to emit photons via an analogous process [BEK77]. In fact, spontaneous Hawking radiation can be viewed as virtual-vacuum photon induced stimulated emission from black holes. In section VII we assume stimulated emission is a universal property of all matter, and extend the concept of stimulated emission to point-like fundamental particles.

To calculate the cross-correlation signal, we assume (similar to section IV.D.1) two unfiltered detectors 1 and 2, both a large distance d from a black-body source, each covering a solid angle $d\Omega$, and separated by a distance much smaller than d (see Fig. B.1). The photon-emission rate per unit solid angle, in an energy slice $d\varepsilon$ wide, heading towards the detector pair is given by [Eq. (IV.B.5) divided by 4π]

$$R = \frac{\sigma_s}{4\pi^3\hbar^3c^2}\frac{\varepsilon^2}{\exp(\varepsilon/T)-1}d\varepsilon\,, \tag{B.1}$$

where σ_s is the cross-sectional area of the black body as viewed from the detector pair. The mean rate of photon detection in each of the detectors is therefore $Rd\Omega$. As in section IV.D.1, we assume that on each photon detection a unit current is generated for a time period dt. The average current (signal) in each of the detectors is given by

$$\overline{S}_i = Rd\Omega dt \tag{B.2}$$

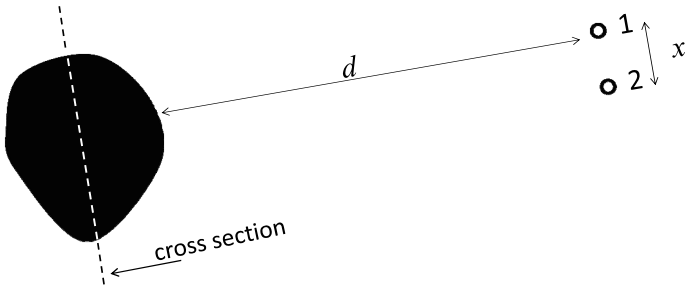

Fig. B.1. Two detectors 1 and 2 observing a black body. The dashed line depicts the cross-sectional area as viewed from the detectors.

The cross-correlation signal associated with accidental coincidences is the rate of observing photons in either detector multiplied by the probability of seeing a coincidence in the other detector within a time window of dt, multiplied by the average cross-correlation signal associated with accidental coincidences $dt/2$ (see section IV.D.1), and is thus given by

$$< S_1S_2 >_A = 2Rd\Omega \times Rd\Omega dt \times \frac{dt}{2} = \left(Rd\Omega dt\right)^2 = \overline{S}_1\overline{S}_2 \tag{B.3}$$

The cross-correlation signal due to real coincidences is more complex. To determine this signal we will first obtain the cross-correlation signal due to events associated with the emission of m correlated photons emitted from the surface of the black body, and then sum over all m. The probability per unit time that exactly m correlated photons are emitted was previously obtained in Appendix A. The rate of emission events containing m correlated photons per unit solid angle is given by

$$R(m) = \frac{\sigma_s\varepsilon^2 d\varepsilon}{4\pi^3\hbar^3c^2}\frac{f^m}{m}\,, \tag{B.4}$$

where, as in Appendix A, $f = \exp(-\varepsilon/T)$. The rate of seeing any one of the m photons in either of the two detectors is given by

$$R(m,\text{seen}) = \frac{f^m\sigma_s\varepsilon^2 d\varepsilon d\Omega}{2\pi^3\hbar^3c^2}\,. \tag{B.5}$$

Upon seeing this photon, the direction back to the source, and therefore the cross-sectional area of the effective aperture, is defined. The probability that one of the other $m-1$ correlated photons becomes the second detection in a real coincidence, in the other detector, is governed by diffraction and given by (similar to that done in section IV.D.1)

$$P_{2^{nd}} = (m-1)\frac{\sigma_s}{\lambda^2}F(r_1,r_2)d\Omega. \tag{B.6}$$

Given the above equations, and assuming dt is much larger than the coherence time $\tau = \hbar/d\varepsilon$, then the cross-correlation signal due to the emission of events involving a photon multiplicity of m is given by

$$< S_1 S_2 >_m = \frac{f^m \sigma_s \varepsilon^2 d\varepsilon d\Omega}{2\pi^3 \hbar^3 c^2}(m-1)\frac{\sigma_s}{\lambda^2}F(r_1,r_2)d\Omega dt \tag{B.7}$$

Summing over all $m > 1$ gives the cross-correlation signal due to all real coincidences

$$\begin{aligned}
< S_1 S_2 >_R &= \frac{f\sigma_s \varepsilon^2 d\varepsilon d\Omega}{2\pi^3 \hbar^3 c^2}\frac{\sigma_s}{\lambda^2}F(r_1,r_2)d\Omega dt\sum_{m=2}^{\infty}(m-1)f^{m-1} \\
&= \frac{\sigma_s \varepsilon^2 d\varepsilon}{4\pi^3 \hbar^3 c^2}\frac{f}{1-f}2(1-f)d\Omega^2 dt^2\,\frac{\sigma_s}{dt\lambda^2}F(r_1,r_2)\sum_{m=2}^{\infty}(m-1)f^{m-1} \\
&= \left(Rd\Omega dt\right)^2 2(1-f)\frac{\sigma_s}{Rdt\lambda^2}F(r_1,r_2)\sum_{m=2}^{\infty}(m-1)f^{m-1} \\
&= \overline{S}_1\overline{S}_2 \cdot 2(1-f)\frac{4\pi^3\hbar^3c^2}{\sigma_s\varepsilon^2 d\varepsilon}\frac{(1-f)}{f}\frac{\sigma_s}{dt\lambda^2}F(r_1,r_2)\sum_{m=2}^{\infty}(m-1)f^{m-1} \\
&= \overline{S}_1\overline{S}_2(1-f)^2\frac{1}{d\nu dt}F(r_1,r_2)\frac{1}{(1-f)^2} = \overline{S}_1\overline{S}_2\frac{\tau}{dt}F(r_1,r_2).
\end{aligned} \tag{B.8}$$

Adding the accidental and real coincidences gives the Hanbury Brown and Twiss effect as given by Eq. (IV.D.1). As in section IV.C.3 and Appendix A, the analysis in this appendix demonstrates that some quantum effects can be obtained semi-classically by the inclusion of stimulated emission.

References

[BEE99] C. W. J. Beenakker, Diffuse Waves in Complex Media, NATO ASI Ser. C, Vol. 531, ed. J.-P. Fouque (Kluwer, 1999), p. 137.

[BEK77] J. D. Bekenstein and A. Meisels, Phys. Rev. **D 15**, 2775 (1977).

[BET44] H. A. Bethe, Phys. Rev. **66**, 163 (1944).

[BET47] H. A. Bethe, Phys. Rev. **72**, 339 (1947).

[BET50] H. A. Bethe, L. M. Brown, and J. R. Stehn, Phys. Rev. **77**, 370 (1950).

[BJO64] J. D. Bjorken and S. D. Drell, Relativistic Quantum Mechanics, McGraw-Hill ISBN 07-005493-2 (1964).

[BOH13] N. Bohr, Philosophical Magazine **26**, 1 (1913).

[BOH39] N. Bohr and J. A. Wheeler, Phys. Rev. **56**, 426 (1939).

[BOR75] M. Born and E. Wolf, Principles of Optics, Pergamon Press, 1975, Chap. VIII.

[BRO92] L. S. Brown, Quantum Field Theory, Cambridge University Press ISBN 0-521-400066 (1992).

[CLE07] B. Cleuren and C. Van den Broeck, Eur. Phys. Lett. **79**, 30001 (2007).

[CRI07] L. C. B. Crispino, E. S. Oliveira, A. Higuchi, and G. E. A. Matsas, Phys. Rev. D **75**, 104012-1 (2007).

[DIR27] P. A. M. Dirac, Proc. Roy. Soc. (London) **A114**, 243 (1927), **A117**, 610 (1928).

[DYS49] F. Dyson, Phys. Rev. **75**, 486 (1949), **75**, 1736 (1949).

[EIN05] A. Einstein, Annalen der Physik **17**, 132 (1905).
[EIN17] A. Einstein, Physik Zeit. **18**, 121 (1917).
[ERL06] J. Erler and P. Langacker, Journ. Phys. G **33**, 119 (2006).
[EVA35] M. G. Evans and M. Polanyi, Trans. Faraday Soc. **31**, 875 (1935).
[EYR35] H. Eyring, Journ. Chem. Phys. **3**, 107 (1935).
[FAB75] R. Fabbri, Phys. Rev. **12**, 933 (1975).
[FAN61] U. Fano, Amer. J. Phys. **29**, 539 (1961).
[FEY49] R. P. Feynman, Phys. Rev. **76**, 749 (1949), **76**, 769 (1949).
[FEY85] R. P. Feynman, QED The strange theory of light and matter, Penguin Books (1985).
[HAN56] R. Hanbury Brown and R. Q. Twiss, Nature **177**, 27 (1956), and
R. Hanbury Brown and R. Q. Twiss, Nature **178**, 1046 (1956).
[HAN11] D. Hanneke, S. Fogwell Hoogerheide, and G. Gabrielse, Phys. Rev. A **83**, 052122 (2011).
[HAU52] W. Hauser and H. Feshbach, Phys. Rev. **87**, 366 (1952).
[HAW74] S. W. Hawking, Nature **248**, 30 (1974).
[HEI25] W. Heisenberg, Z. Physik **33**, 874 (1925).
[HIN06] I. Hinchliffe, Journ. Phys. G **33**, 110 (2006).
[IRA08] Z. Irahharten et al., IEEE International Conference on Communication, 2008, pg. 4872.
[JEN14] U. D. Jentschura and I. Nandori, Eur. Phys. J. H, **39**, 591 (2014).
[KAR52] R. Karplus, A. Klein, and J. Schwinger, Phys. Rev. **86**, 288 (1952).
[KEM33] E. C. Kemble and R. D. Present, Phys. Rev. **44**, 1031 (1933).
[LAM47] W. E. Lamb and R. C. Retherford, Phys. Rev. **72**, 241 (1947).
[LEI90] J. R. Leigh, Phys. Rev. C **52**, 3151 (1995).
[LES90] J. P. Lestone, PhD thesis, Australian National University, Canberra, 1990.
[LES97] J. P. Lestone et al, Jour. Phys. G **23**, 1349 (1997).
[LES07] J. P. Lestone, arXiv:physics/0703151 (2007).
[LES08] J. P. Lestone, Int. Jour. Mod. Phys. E **17**, 323 (2008).
[LES08b] J. P. Lestone, Mod. Phys. Lett. A, **23**, 1067 (2008).
[LES09] J. P. Lestone and S. G. McCalla, Phys. Rev. C **79**, 044611 (2009).
[LES16] J. P. Lestone, Nucl. Data Sheets, **131**, 357 (2016).
[MOH15] P. J. Mohr et al, http:/physics.nist.gov/constants (2015), National Institute of Standards and Technology, Gaithersburg, MD 20899, USA.
[PAG76] D. N. Page, Phys. Rev. D **13**, 198 (1976).
[PAU] Writings on Physics and Philosophy Quotes by Wolfgang Pauli, @ www.goodreads.com.
[PLA01] M. Planck, Annalen der Physik **4**, 553 (1901).
[PRU56] E. M. Purcell, Nature **178**, 1449 (1956).
[SCH26] E. Schrödinger, Phys. Rev. **28**, 1049 (1926).
[SCH48] J. Schwinger, Phys. Rev. **73**, 416 (1948), **74**, 1439 (1949), **76**, 790 (1949).
[SOM16] A. Sommerfield, Annalen der Physik **51**, 1 (1916).
[TOM46] S. Tomonaga, Prog. Theor. Phys. **1**, 27 (1946).
[UEH35] E. A. Uehling, Phys. Rev. **48**, 55 (1935).
[WEI37] V. Weisskopf, Phys. Rev. **52**, 295 (1937).
[WEL48] T. A. Welton, Phys. Rev. **74**, 1157 (1948).